MATERIALS CHEMISTRY
FRONTIERS

REVIEW

Cite this: *Mater. Chem. Front.*, 2019, **3**, 2571

Frontiers in carbon dots: design, properties and applications

Zeyu Li, [a] Ling Wang, *[a] Yu Li, [abc] Yiyu Feng [abc] and Wei Feng *[abcd]

Received 25th June 2019,
Accepted 18th September 2019

DOI: 10.1039/c9qm00415g

rsc.li/frontiers-materials

Carbon dots (CDs), which are emerging as a novel class of carbon-based functional nanomaterials, can be fabricated from various carbon-based materials such as graphite, activated carbon, carbon nanotubes and many other organic materials. Recently, researchers have paid attention to emerging CDs and investigated their application prospects in a variety of fields, including optical, energy and biomedical technologies. In this review, we provide an up-to-date account of the design, preparation, fundamentals and applications of functional CDs. We begin with an overview on the synthetic methods of novel CDs, including "bottom-up" and "top-down" approaches, post-synthetic modification and functionalisation, through which the diverse properties of CDs such as optical, dispersibility and biocompatibility properties are introduced. We then showcase the applications of advanced CDs in different fields, including optical applications (data security, sensors, light-emitting diodes, and chiral), energy applications (photocatalysts, solar photovoltaics, supercapacitors, and lithium-ion batteries) and promising biomedical applications (bioimaging and nanomedicine). We discuss the fundamental design ideas of such emerging and unique CDs, introduce their synthetic strategies and emphasise their significant applications. This review is expected to provide significant impetus towards the rapid expansion of this new materials field which is rooted in materials chemistry. The fields covered include physics, chemistry, biology, nanotechnology, energy, polymers, device engineering and other interdisciplinary areas.

[a] *School of Materials Science and Engineering, Tianjin University, Tianjin 300072, P. R. China. E-mail: weifeng@tju.edu.cn, lwang17@tju.edu.cn; Fax: +86 22 27404724; Tel: +86 22 28578269*
[b] *Collaborative Innovation Center of Chemical Science and Engineering, Tianjin 300072, P. R. China*
[c] *Key Laboratory of Advanced Ceramics and Machining Technology, Ministry of Education, Tianjin 300072, P. R. China*
[d] *Tianjin Key Laboratory of Composite and Functional Materials, Tianjin 300072, P. R. China*

Zeyu Li

Zeyu Li received his BS degree in Chemistry from Zhengzhou University (China) in 2015 and completed his MS degree under the supervision of Prof. Kun Dai at Zhengzhou University (China) in 2017. He is now pursuing PhD under the tutelage of Prof. Wei Feng at the School of Materials Science and Engineering, Tianjin University. Currently, his research is focused on carbon dots and solid polymer electrolytes.

Ling Wang

Ling Wang is a full professor at Tianjin University, Tianjin, China. He received his PhD degree in Materials Science from the University of Science and Technology Beijing (China). From October 2013 to September 2018, he worked as a postdoctoral research fellow at the Advanced Materials and Liquid Crystal Institute of Kent State University (USA) and the Artie McFerrin Department of Chemical Engineering at Texas A&M University (USA), respectively. His research interests include design, synthesis and properties of active soft materials, bioinspired materials and functional nanomaterials, as well as their emerging applications in diverse fields ranging from soft robotics, adaptive camouflage, smart windows to energy and safety issues.

1. Introduction

Carbon materials have been utilised in various disciplines, including chemistry, engineering, biomedical science and so on.[1] Many forms of carbon materials exist in nature, and carbon-based materials play a key role in the development of nanomaterials science. From traditional 3D graphite[2,3] to new carbon nanomaterials such as fullerenes,[4,5] 1D carbon nanotubes (CNTs)[6–9] and 2D graphene,[10–12] fundamental research on new carbon materials and their applications has always been a hotspot in the fields of physics, chemistry, materials and other interdisciplinary areas. For example, graphene and CNTs, which display tuneable mechanical, electronic, optical and biocompatibility properties, have attracted much attention in the past few years. In more recent times, a new type of 0D structure and luminescent carbon material has received wide attention, namely, carbon dots (CDs), which are a type of nanoparticle with quasi-spherical morphology and nanoscale characteristic sizes (<10 nm). The amorphous and nanocrystalline nuclei in CDs are mainly composed of sp^3 hybridised carbon inserts of graphene, graphene oxide sheets and diamond-like carbon or sp^2 carbon with graphitic or turbostratic carbon. In 2004, CDs were discovered as a by-product during the preparation of single-walled CNTs (SWCNTs).[13] Since then, the research on CDs has made rapid progress (Fig. 1). In 2006, the first synthesis was carried out; in this study, surface passivation was first applied to CDs to improve their surface character and photoluminescence (PL).[14] In 2007, Liu *et al.* first reported the fabrication of small (<2 nm) multi-coloured fluorescent CDs from the combustion soot of candles, and purified CDs were used in polyacrylamide gel electrophoresis. This is the first attempt at employing the bottom-up approach to prepare CDs and expanding the sources of CDs from inorganic to organic materials.[15] In 2009, CDs were successfully used in *in vivo* imaging, and this work confirmed the biomedical applications of CDs.[16] In 2013, polymers were used for the first time to fabricate CDs; this achievement signified an extension of the range of synthetic precursors of CDs from micromolecules and inorganic carbon materials to polymers and of the portfolio from graphite and micromolecules to include crosslinked polymeric materials.[17] Nowadays, researchers are pursuing the idea of accurately controlling the structure and morphology of CDs such as chiral CDs (fabricated from chiral precursors) and triangularly shaped CDs.[18,19]

Compared with those of traditional quantum dots (QDs),[20–22] CDs exhibit the properties of high luminescence, excellent biocompatibility, low toxicity and low cost, which endow them with the potential for application in different fields, such as optoelectronics and biomedical applications. In addition, as a newly developing nanomaterial, CDs reveal the potential for application in energy storage and photovoltaic fields as a dopant (as a donor/acceptor of electrons) owing to their charge injection/separation properties.[23–25] Consequently, the exploration for simple and efficient methods to prepare high-performance CDs has become one of the focuses of researchers. Although researchers have explored CDs both extensively and intensively, it is still a major challenge to quantitatively design CDs with unique physical and chemical properties because of their composite chemical structure. Furthermore, contradictory experimental results have been reported by different research groups on the PL behaviour, which include the emission wavelength (λ), quantum yield (QY), dispersion, ultraviolet-visible absorption (UV-visible absorption), and some phosphorescence properties.[14,26–29] To date, three kinds of PL mechanisms have been proposed on the origin of fluorescence in CDs: (1) core-state emission, due to a few defects and functional groups which induce perfect carbon crystal core fluorescence emission;[30,31] (2) surface-state emission, due to coordination bonds on the carbon backbone and the adjacent chemical groups, which determine the fluorescence emission;[32] and (3) molecular fluorescence, due to the

Yiyu Feng

Yiyu Feng is a professor in the School of Materials Science and Engineering at Tianjin University. He obtained his PhD from Tianjin University in 2009 and held an academic position at Tianjin University. He has authored and co-authored over 100 academic articles and reviews. Currently, his research is focused on carbon-based materials or composites for solar-thermal fuels, interfacial heat dissipation and structural self-healing.

Wei Feng

Wei Feng is a professor at the School of Materials Science and Engineering in Tianjin University. He obtained his PhD degree from the Xi'an Jiaotong University (China) in 2000. Then, he worked at Osaka University and Tsinghua University as a JSPS fellow and postdoctoral researcher, respectively. In 2004, he became a full professor at Tianjin University. He has obtained the support of the National Science Fund for Distinguished Young Scholars in China. His research interests include photo-responsive organic molecules and their derivatives, thermal-conductive and high-strength carbon-based composites, and two-dimensional fluorinated carbon materials and polymers.

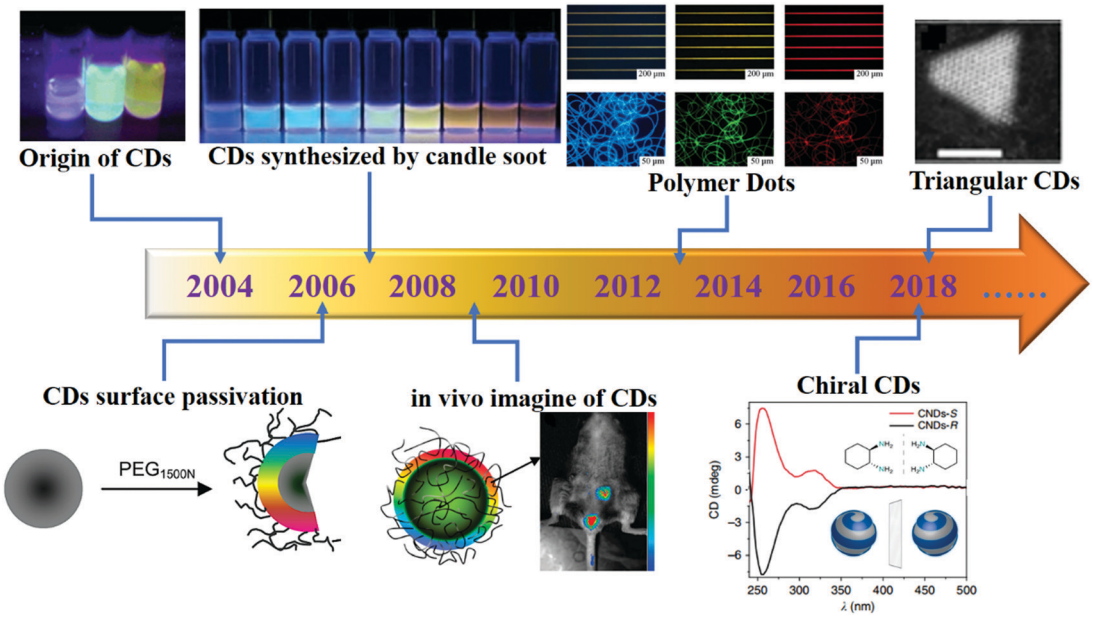

Fig. 1 Milestones in the development of CDs. Reprinted with permission from ref. 13–19. Copyright 2004, 2006, 2009, American Chemical Society. Copyright 2007, 2013, Wiley-VCH Verlag GmbH & Co. KGaA. Copyright 2018, Nature Publishing Group.

fluorescence of the molecules and the by-products formed during the synthesis process which induce fluorescence emission.[33,34] Multiple factors influence the disparate properties obtained from experiments, such as λ being mainly affected by the surface groups and their sizes and other properties (*e.g.* QY and phosphorescence) resulting from heteroatom doping and modification of the functional groups. Consequently, clarifying the relationship between the physical and chemical properties and the morphology and structure of CDs will have a far-reaching impact on their applications.

Tuneable PL, as the most fascinating property, has been of interest to researchers. It is worth mentioning that researchers have prepared full-coloured CDs from the blue to the near-infrared (NIR) fluorescence region by diverse methods; the QYs of such CDs exceeded 80%.[35] Hence, CDs can also be employed in the optics field, which includes information encryption,[36,37] light-emitting diodes (LEDs),[38,39] sensors,[40,41] photocatalysts[42] and chiral photonics.[43,44] On the other hand, various unique characteristics of CDs which were determined reveal that they can replace the traditional QDs and organic dyes applied in *in vitro* and *in vivo* fluorescence imaging as fluorescent nanoprobes. Four reasons can be attributed in this regard: (1) CD biocompatibility, which suggests that cells or organisms can live in a CD environment. (2) CD solubility and stability; abundant hydrophilic groups such as amino and carboxyl groups which help CDs display the ability to dissolve and disperse in water or organic solvents. (3) CD photostability; the resistance to photobleaching suggested that CDs can maintain their photostability under a high radiation intensity and long-time light conditions. (4) CD cost efficiency; their low cost and the convenience of preparation result in a very high economic benefit.[45] Therefore, it is a feasible strategy to apply CDs in the biomedical field, such as for target-specific bioimaging[46–48] and in nanomedicine.[49,50] Finally, CDs can often display a high optical absorptivity across much of the visible light region, which renders them a possible alternative sensitiser. In addition, owing to the large π-electron network (sp^2 core) within crystalline CDs, they can also function as electron acceptors/donors and conductive intermediates for electron transport, or form heterojunctions at sites of charge separation, which allow them to serve as charge carrier sources, funnels, bridges, *etc.* Consequently, CDs have been applied in the energy field, especially in solar photovoltaics,[24,25,51] supercapacitors[52–54] and lithium-ion batteries (LIBs).[55–57]

In this review, we first discuss the fundamentals of CDs, including the synthetic strategies and basic properties. Then, we highlight the important applications of CDs in diverse fields, including optical (data security, sensors, light-emitting diodes, chiral), energy (photocatalysts, solar photovoltaics, supercapacitors, LIBs) and promising biomedical applications (bioimaging and nanomedicine). We also present the fundamental ideas of designing such emerging and unique CDs, introduce their synthetic strategy and emphasise their significant applications. Finally, we discuss the prospects and challenges of CDs, including their potential applications and future development trends. It is worth mentioning that we are not going to provide a comprehensive list of all the applications of CDs, rather the aim is to briefly introduce those fields where CDs reveal particularly outstanding performances, according to some of the latest results. In addition, we hope to further understand the physical and chemical properties of CDs and offer valuable insights into the selection of their applications.

2. Fundamentals of CDs

As a kind of nanoparticle, CDs have been extensively researched in terms of their synthesis methods. At present, the preparation of CDs can be mainly divided into two subclasses: bottom-up

and top-down methods. However, neither method can precisely control the physicochemical properties of CDs. Still, researchers identified some factors that influence the properties of CDs. For instance, the size of CDs can be regulated by controlling the reaction condition and time. In addition, surface groups can be added to CDs by passivation. Hence, it is very important to identify an effective synthesis strategy to achieve precise control in the performance of CDs. In this section, we briefly summarise some of the representative synthetic strategies and CD properties. We also analyse the relationship between the physics and chemical structure and the electronic, electrochemical and optical properties.

2.1 Synthetic strategies of CDs

CDs were first discovered in 2004 from an unrelated synthetic process.[13] After that, diverse synthesis pathways have been identified to fabricate CDs. It has become the common goal of researchers to find CDs with the characteristics of simple synthetic methods, uniform size and structure, diverse functions and gratifying economic benefits. According to the growth process during the preparation process of CDs, the synthetic strategies are generally divided into two subclasses, namely "top-down" and "bottom-up" (Fig. 2a).[28] In 2007, Sun *et al.*[14] used organic molecules for surface passivation of CDs. Then, this surface modification method was proposed and widely used for CDs. Moreover, a large number of studies proved that heteroatom doping can also effectively functionalise CDs.

2.1.1 Top-down methods. The CDs synthesised by the top-down approach employed macroscopic carbon materials such as graphite, graphene, CNTs and fullerene as the carbon sources. Laser ablation,[14] electrochemical,[58,59] arc discharge[13] and chemical oxidation methods are included in this group of methods.

The first synthesis process used for the preparation of CDs was arc discharging. Here, tubular carbon and CDs were obtained from crude soot and SWCNTs, respectively.[60,61] Moreover, laser ablation is widely applied for the preparation of CDs because of the advantages of easily controllable morphology and size, high purity and good reproducibility. Sun *et al.*[14] reported a type of CD which was produced by laser ablation of a carbon target in an atmosphere of water vapour with argon. Nguyen *et al.*[62] fabricated CDs by using the femtosecond laser ablation method; they found that the CD size increased with laser fluence and spot size. Further, this phenomenon is not unique. Hu *et al.*[63] also found in 2011 that the size of CDs is dependent on laser width. They explained this phenomenon based on the instant when the energy of a femtosecond pulse is released to the precursor material, when the high-temperature high-pressure plasma plume produced by the ionisation caused by multi-photon absorption induces a Coulomb explosion and

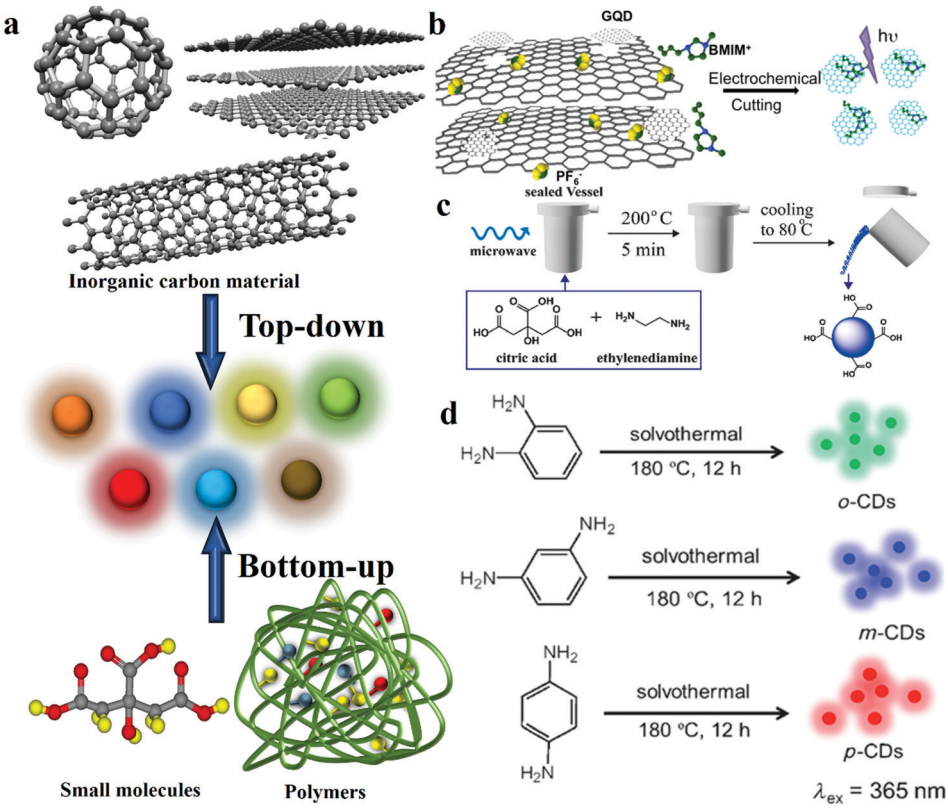

Fig. 2 Schematic representations of the different approaches of preparing CDs. (a) CD synthetic strategies: bottom-up and top-down approaches. (b) GQD synthesis from 3D graphene. Reprinted with permission from ref. 70, Copyright 2014, Wiley-VCH Verlag GmbH & Co. KGaA. (c) CD synthesis *via* microwave-assisted heating with controllable temperature. Reprinted with permission from ref. 74, Copyright 2015, The Royal Society of Chemistry. (d) Hydrothermal preparation of RGB PL CDs. Reprinted with permission from ref. 29, Copyright 2013, Wiley-VCH Verlag GmbH & Co. KGaA.

cavitation bubbles are formed in the system after cooling, which result in the carbon nanoclusters having larger space sites for developing.[64–66] It indicates that the CD size can be tuned by controlling the laser parameters. Although the laser ablation method offers the advantage of size control, its high cost and complicated operation limit the possibility of large-scale production.

Moreover, Zhou *et al.*[67] first demonstrated a novel approach for preparing CDs by electrochemical oxidation treatment of multi-walled carbon nanotubes (MWCNTs). Compared with laser ablation, the electrochemical method also offers the merits of controllable size, high purity and good reproducibility. Shinde and co-workers[68] synthesised size-selective graphene quantum dots (GQDs) by the electrochemical method with MWCNTs. They precisely regulated the height and width of GQDs by changing the reaction time and temperature. The results revealed that the reaction time and temperature are inversely proportional to the size of GQDs. Ming *et al.*[69] produced CDs by the electrochemical approach. It is worth mentioning that the only constituent of the electrolyte is pure water, which does not offer any chemical assistance. They inserted a graphite rod into ultrapure water as the anode, and placed another graphite rod as the counter electrode (CE). Then, a direct voltage of 15–60 V was applied to this system while stirring continuously for 120 h to finally obtain CDs. This approach demonstrated the possibility of continuously producing environmentally friendly CDs. In addition to using graphite and CNTs as the carbon sources, the electrochemical cutting method of using graphene as a precursor to prepare GQDs has been reported.[70] A type of GQD was prepared by the electrochemical strategy by using monolithic 3D graphene, which was grown by chemical vapour deposition by utilising the room temperature ionic liquid, 1-butyl-3-methylimidazolium hexafluorophosphate (BMIMPF6) in acetonitrile, as the electrolyte (Fig. 2b). The average thickness of the GQDs is $\approx$1.25 nm, and the GQDs reveal a narrow plane size of average lateral diameter $\sim$3.0 nm.

Researchers also used the strong acid-based oxidation method to prepare CDs. In this approach, they selected concentrated nitric acid or sulfuric acid. For example, Ye *et al.*[71] reported a facile approach of synthesising tuneable GQDs from various types of coals. They produced three types of GQDs from bituminous coal (b-GQDs), coke (c-GQDs) and anthracite (a-GQDs). They added the three types of coals to concentrated sulfuric acid and nitric acid, which was followed by heat treatment at 100 or 120 °C for 24 h. Among the three GQDs, the average size of b-GQDs is the smallest, being 2.96 $\pm$ 0.96 nm, whereas the sizes of a-GQDs and c-GQDs are 29 $\pm$ 11 and 5.8 $\pm$ 1.7 nm, respectively. They used this method to produce GQDs isolated from coal, the yields of which can reach 20%. Compared with the other top-down methods, chemical oxidation is easier to perform and offers greater potential for large-scale production. Further, the abundance of the source implies that the CDs prepared by this approach can be applied as inexpensive additives in structural composites.

2.1.2 Bottom-up methods. In CDs, the PL behaviour can be traced to the ''quantum effects'', and the fluorescence properties are associated with the particle surfaces. Accordingly, the synthesis schemes for the modification of the CD surface play a central role. For the CDs synthesised by the top-down approach, surface passivation has been achieved with the help of many polymers, such as poly(ethylene glycol) (PEG) and propionylethylenimine-co-ethylenimine (PPEI–EI).[72] After the surface passivation process, ''defects'' or functional groups are formed on the CD surface, and the generation of these structures affects the physical properties of CDs, such as lyophobic–hydrophilic transfer. In order to more easily prepare functional CDs from readily available precursors, a one-step method has been demonstrated through the bottom-up approach. The bottom-up approach is used to mainly synthesise CDs from organic materials, and quantum-sized CDs are formed *via* the polymerisation reaction of organic molecules. There are a variety of techniques which belong to this approach, such as the hydrothermal,[17,73] microwave-assisted,[74–76] ultrasonic[77,78] and template methods.[79,80]

Microwave-based synthesis has been employed in CD fabrication. Fig. 2c depicts a microwave-assisted synthesis process of producing CDs by using citric acid (CA) and ethylenediamine (EDA).[74] A CA and EDA water solution was transferred to a sealed digestion vessel and placed inside a microwave digestion furnace at 200 °C for 5 min; then, the system was naturally cooled to 80 °C and, after dialysis, CDs were obtained. The QY of fluorescent CDs is up to 96% by this method, and the CDs show a uniform dispersion and a relatively narrow size distribution of 2–6 nm, with an average size of 3.5 nm.

The CDs prepared by the hydrothermal carbonisation approach offer the advantages of low cost, environmental friendliness and extensive precursor sources, therefore, it is popular with researchers. CDs were produced by the reaction of an organic precursor solution in a sealed container at a high temperature and pressure. Lin's group[29] reported the fabrication of highly photoluminescent multi-coloured CDs by the hydrothermal method. The CDs were prepared with CA and nitrogen dopants were added in different proportions to adjust the QY and emission wavelength of the CDs under 365 nm excitation. Besides, Yang' group reported CDs with 80% QY under optimal reaction conditions when using EDA as the nitrogen dopant. Transmission electron microscopy (TEM) images show CDs without apparent aggregation and well-dispersed particles of diameters 2–6 nm. The average height of the CDs was obtained as 2.81 nm through AFM. In addition, chocolate,[81,82] fruit,[27,83,84] hair[85] and even rubbish[86–89] can be used as precursors to prepare CDs by the hydrothermal method. The abundance of the source and the simple synthesis process offer the advantage of low cost. However, the complex purification process in this approach suggests that it cannot be applied to large-scale production.

Moreover, novel bottom-up approaches have been reported, such as electrochemical and template methods. Novel electrochemical preparation of solid-state CDs was reported by Niu and co-workers.[90] The growth of CDs *via* the electrochemical approach involved the use of two platinum sheets as the working and counter electrodes and $BMIMPF_6$/acetonitrile as the electrolyte; the reaction process consisted of applying a DC voltage of 15 V between the two electrodes for 10 h. The QY of the CDs

produced was 11.6%, and a narrow size distribution (2.0–4.4 nm) was observed. The CDs exhibited a distinct crystal structure, with a lattice spacing of around 0.208 nm, which agrees well with both the (103) diffraction planes of diamond-like (sp^3) carbon and the (102) diffraction planes of sp^2 graphitic carbon. Specifically, compared with the traditional top-down electrochemical preparation method, this approach offers the merits of absorption on the surfaces of the electrode materials and purification by simple vacuum filtration, owing to the use of carbon-free electrodes and an ionic liquid as the carbon source to obtain the final products. Thus, this method offers the potential for application in large-scale production. In addition, in order to solve the problem of CD dispersion being difficult to achieve, Kwon *et al.*[79] realised nearly monodisperse CDs by the emulsion-templated carbonisation method. The CDs were fabricated by carbonisation of glucose dispersed in water-in-oil emulsions. In this work, the hydroxyl groups in the carbohydrate were good for stabilising the emulsion and preventing flocculation. The coating effect of the emulsion particles on glucose led to the formation of monodisperse carbohydrates and prevented agglomeration. The monodisperse structure was verified by TEM (an average diameter of 1.403 nm), and the lattice spacing of 0.25 nm confirmed the formation of a graphitised structure on the (100) crystal facets. Owing to the almost monodisperse characteristic, a high QY of 53% of the CDs was recorded for 420 nm excitation.

2.1.3 Post-synthetic modification and functionalisation. In order to further regulate the properties of CDs, their structure in general can be modified through several post-synthetic strategies, such as heteroatom doping and surface modification.

Heteroatom doping is widely used for manipulating the properties of CDs. CDs can facilely combine with the heteroatoms (*e.g.* nitrogen, boron, sulfur and fluorine) of a reactant. The one-pot method is a popular technique for preparing heteroatom-doped CDs. For example, Zhang *et al.*[91] synthesised nitrogen-doped fluorescent CDs by using CCl_4 as the carbon source and $NaNH_2$ as the dechlorination reagent and nitrogen source. The emission wavelength of the obtained CDs can be adjusted from blue to yellow by controlling the amount of doped nitrogen. On the other hand, multiatom doping can also be employed in CDs. For example, nitrogen and sulfur co-doped CDs were reported by Li and Yu's group.[92] CA served as the carbon source, and L-cysteine provided the nitrogen and sulfur. The obtained CDs exhibited a QY as high as 73%, which was due to a synergistic effect between the doped nitrogen and sulfur atoms. Moreover, Fei *et al.*[93] reported a type of boron- and nitrogen-doped GQDs (BN-GQD); ammonia and boric acid were used as the nitrogen and boron sources, respectively (Fig. 3a). Although the modification of CDs by heteroatom doping offers the advantage of simple preparation, the chemical structure of the product is unclear owing to the uncontrollability of the doping process, which is contrary to the original intention of accurately designing a CD structure. Consequentially, a new method had to be sought to prepare CDs by controlled doping. On the other hand, the surface passivation and/or functionalisation (SPF) strategy is more controllable owing to the maturity of

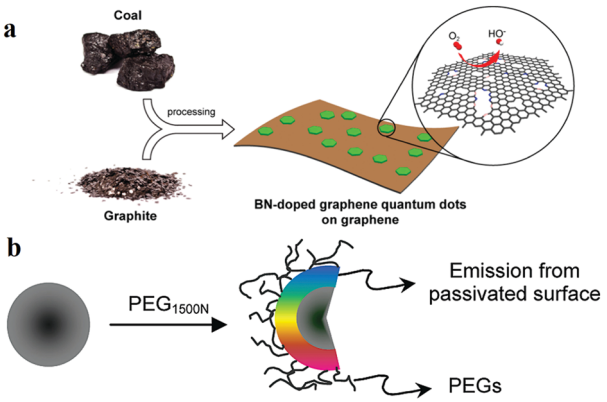

Fig. 3 Schematic representations of the heteroatom doping and surface passivation approaches of CD functionalisation, reprinted with permission from ref. (a) Illustration of the preparation procedure for the BN-GQD/graphene nanocomposite, reprinted with permission from ref. 93, Copyright 2014, American Chemical Society. (b) Functionalisation of CD surfaces with PEG, reprinted with permission from ref. 14, Copyright 2006, American Chemical Society.

the organic reactions involved. It is ascribed to the fact that the functional groups of CDs can be more easily eliminated, formed or converted by SPF. In order to modify and passivate the surface, small molecules and polymers were selected as the modification agents. Passivation is an effectivity method to localise the e–h pairs of CDs in the surface states. In simple terms, it is a process of eliminating the dissipation of photosensitive carriers from the surface, thereby achieving a more efficient radiation recombination and improving the PL performance of CDs. Therefore, unlike bare CDs, the CDs subjected to passivation display higher optical activities and remarkable PL properties, which are observed over a wide spectral range, from the visible to the NIR region. Sun *et al.*[14] first reported that CDs subjected to surface passivation reveal strong PL properties. In this work, the diamine-terminated oligomeric PEG_{1500N} served as the surface passivating agent (Fig. 3b). Moreover, they also observed that PPEI–EI, when used for surface passivation, generated photoluminescent CDs which were similar to PEG-CDs. On the other hand, semiconductor salts such as ZnS and ZnO were used as dopants in surface-passivated CDs. Sun and colleagues[94] revealed that ZnO- or ZnS-doped CDs, upon passivation with PEG_{1500N}, could reveal enhanced QYs. In this system, they observed the formation of semiconductor salt lattices on the surface of the CDs, and the improvement in the PL property may be attributed to the promotion of "defect" formation on the surface in the presence of the semiconductor salts.

2.2 Basic properties of CDs

CDs exhibit complex microstructures, crystallinity and diverse sizes, therefore, it is necessary to research the underlying relationship between the structure and the properties of CDs. Several key CD properties have been reported, including UV-visible absorbance, luminescence, dispersibility, biocompatibility and toxicity.

2.2.1 UV-visible absorbance and stability. In order to better investigate the luminescence properties of CDs, researchers need to study the UV-visible absorbance in detail. Although the CDs obtained through different methods exhibit different chemical structures, most of them display UV-visible absorption, which has been confirmed by numerous studies. However, the positions of the UV absorption peaks are quite different. Tang *et al.*[95] prepared GQDs *via* a microwave-assisted hydrothermal approach by using glucose. The GQDs demonstrated deep UV emission, and doubly strong UV absorbance peaks were obtained at 282 and 228 nm; the change in the intensities of the peaks showed the common trend, increasing exponentially as the reaction time increased. At the same time, the influence of solution concentration and microwave irradiation power on the growth of GQDs could also be proved based on the contrasting UV absorption spectra. For example, when the reaction time increases, red-shift of the absorption edge occurs, but the position of the peak does not change. The origins of these peaks are related to the π electron transitions in the oxygen-containing GQDs. The 228 nm absorption peak corresponded to the π–π* transition of the C=C bond, whereas the absorption at 282 nm is due to the n–π* transition of C=O. In addition, Li *et al.*[96,97] prepared two types of photoluminescent CDs by the hydrothermal approach by using CA and urea which were then treated with an aqueous alkali (NaOH or KOH) solution to obtain metal-cation-functionalised CDs1; they were further treated with HCl to obtain CDs2. Owing to the large conjugated sp^2 structure of the particles, the UV-visible spectrum of CDs1 reveals a distinct visible absorption peak at 540 nm. CDs2 also exhibits a visible light absorption band at the same position as CDs1, though the wave shoulder is broader. It can be proved that the UV-visible absorbance is affected by the presence of charged functional groups on the surface of CDs.

Photobleaching is an important optical property of CDs; materials with low photobleaching permit long-term real-time imaging. Compared with those of traditional QDs, CDs display higher resistances to photobleaching and higher photostability. The anti-photobleaching property of CDs is affected by the reaction time and temperature during the synthesis process. For example, Wang *et al.*[98] found that the QY of CDs composed of p-conjugated domains (carbon core) and low-molecular weight fluorophores decreased with the increase in the reaction temperature and time, while the anti-photobleaching property increased, due to the low molecular weight fluorophores combining with the p-conjugated structure during the reaction process. The larger p-conjugated domains formed by surface-bound fluorophores display a stronger ability to dissipate the absorbed UV energy and protect the system from photochemical damage. Furthermore, it was found that pyridone-like structures may be the most effective in offering protection against photobleaching of CDs. This provides a basis for designing CDs with anti-photobleaching characteristics through structural control. In addition, Xiong *et al.*[99] showed that CDs with higher degrees of carbonisation display greater stabilities when subjected to photobleaching, which is due to these CDs receiving increased photochemical damage protection from the carbon matrix.

2.2.2 Fluorescence. The light emission properties of CDs are the most fascinating in CD research, and have therefore attracted attention. There has been a rapid expansion of research on the PL[100,101] and up-converted PL (UCPL)[78,102,103] of CDs; these two emission behaviours are followed by Stokes shift and anti-Stokes shift, respectively. The multiple luminescence behaviours render CDs a widely applied material in the fields of photoelectricity, energy and biology. The PL emission wavelength is longer than the excitation wavelength. The PL of CDs can be divided into two subclasses: fluorescence and phosphorescence. UCPL is different from ordinary PL, in that the energy corresponding to the emission wave is higher than that corresponding to the excitation wave; as a result, the emission wavelength is shorter than the excitation wavelength. Early studies on the UCPL of CDs used monochromatic light emitted from a fluorescence spectrophotometer (in which a xenon lamp was used as the light source without a filter) for testing. In this case, the second-order diffraction of $\lambda/2$ wavelength (which always coexists in the excitation radiation of wavelength λ) due to conventional PL was always misinterpreted as UCPL.[78,104–107]

As a very attractive light-emitting material, the fluorescence properties of CDs suggests that it has the potential to replace the traditional organic dyes and QDs. The QY and the emission wavelength are two important parameters which describe the fluorescence properties of CDs.[108] In addition, from the viewpoint of structure, there is no doubt that the size, defects, functional groups and even phase state determine the fluorescence characteristics of CDs. Although the initial CD QY reported was only about 6%,[67] appropriate synthetic strategies can be used to improve this value. On the other hand, with regard to the emission wavelength, most of the existing CD emission wavelengths show strong excitation dependences *e.g.* when CDs are excited with UV light, the emission is intense in the blue-to-green spectral region.[109] Thus, by importing special structures such as those based on fluorine- or nitrogen-containing groups[110,111] and controlling the oxygen content of the CD surface, the emission wavelength can be tuned.[112–114]

Several recent studies reported the influence of some structures on the fluorescence of CDs. Ding *et al.*[114] reported CDs with a QY of 35% which were fabricated by the hydrothermal approach, the PL of which can be tuned by the addition of oxygen atoms. They proposed that the luminescence of CDs is mainly caused by the conjugated carbon atoms and bonded oxygen atoms on the surface. Oxygen content played a central role in regulating the band gap between the highest occupied molecular orbital (HOMO) and the lowest unoccupied molecular orbital (LUMO) of this structure.[115] Through experiments, with the increase in the surface oxygen content in the system, the band gap was found to gradually decrease, and a red-shift of the emission peak from 400 to 625 nm was observed (Fig. 4a). The mechanism of surface state emission was also verified by Bao *et al.*[116] They prepared CDs by using nitric acid oxidised carbon fibres. The surface state and the size of the CDs were adjusted by controlling the reaction time, HNO_3 concentration

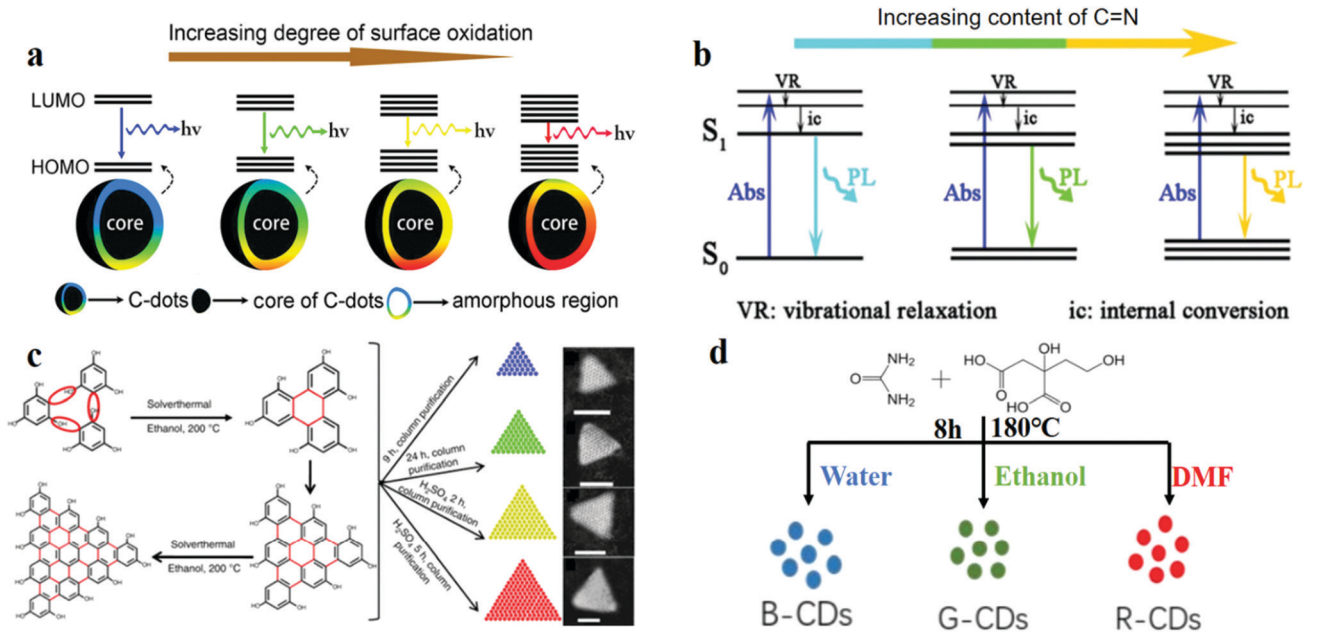

Fig. 4 Model for controlling CD fluorescence: surface, functional groups, size and solvent. (a) Red shift of the emission from CDs occurs with the increase in the degree of surface oxidation. Reprinted with permission from ref. 114, Copyright 2016, American Chemical Society. (b) Energy structures and PL emission processes; the band gap narrows for increasing C═N content on the CD surface. Reprinted with permission from ref. 117, Copyright 2017, The Royal Society of Chemistry. (c) Solvothermal route to triangular CDs, which reveal greater red-shifted emissions for increasing sizes of the CDs. On the far right are the SEM images of the CDs. Reprinted with permission from ref. 19, Copyright 2018, Nature Publishing Group. (d) Preparation of CDs by solvothermal treatment with three different solvents. Reprinted with permission from ref. 118, Copyright 2017, IOP Publishing.

and reaction temperature. The following conclusions were drawn: (1) Extension of the reaction time increases the degree of surface oxidation, which results in a longer emission wavelength. (2) A high HNO_3 concentration and a short reaction time result in a long emission wavelength. Moreover, Han *et al.*[117] explored the relationship between the surface-state energy gap and fluorescence. Three types of polymer CDs (PCDs) were prepared by autopolymerisation and self-oxidation. XPS characterisation revealed that for the three types of PCDs, the C═N contents were 59.29%, 20.11% and 13.83%, and the red-shift of the PL spectrum increased with the increase in the content of C═N on the PCD surfaces. This is reasonable because the band gap narrows with an increase in the C═N content on the PCD surface. Increasing the number of C═N on the PCD surface introduces additional new energy levels in the electronic structures of the PCDs, which induce more electronic transitions and thus produce a red-shift of the PL spectrum (Fig. 4b). Zhu *et al.*[118] proposed that a synergistic effect between C═O and C═N led to the fluorescence of CDs. They designed and fabricated three types of CDs by using three different solvents (water, ethanol, and dimethylformamide) through the hydrothermal method (Fig. 4d). The results were verified using the XPS data and the fluorescence spectra. Particle size also plays an important role in determining the band gap, which further affects the shift in the fluorescence wavelength. For example, specially shaped CDs with multi-coloured narrow bandwidth emission were prepared by Fan's group.[19] Their TEM image showed that the CDs were triangular, and the QY of the CDs was up to 54–72%. They designed and synthesised four sizes of triangular CDs. Symmetric phloroglucinol (PG) was chosen as the precursor. In the cyclisation reaction, the active –H and –OH groups in three adjacent PG molecules form a six-membered ring. Bright multi-coloured emissions of red (R), yellow (Y), green (G) and blue (B) are observed for gradually decreasing sizes from 3.9 to 3.0, 2.4 and 1.9 nm (Fig. 4c), respectively. The band gap becomes narrow with the increase in the particle size, then red-shift of the fluorescence occurs.[29,119,120]

2.2.3 Phosphorescence. Room temperature phosphorescent (RTP) materials find widespread applications in bioimaging, sensing and light-emission.[121] However, traditional RTP materials, which are inorganic or metal complexes, are limited in their applications owing to their high toxicities and high prices.[122–124] Therefore, inexpensive and less toxic RTP materials display large potential for application. Although RTP properties have been revealed in rare pure organic compounds, the short lifetimes and low intensities have limited their development.[125–127] In recent years, researchers have produced high-strength long-life CD RTP materials.[128–134] Deng *et al.*[129] first reported the RTP phenomenon by dispersing CDs in a polyvinyl alcohol (PVA) matrix. A sub-second-order phosphorescent lifetime was observed in the water-soluble CDs. The CDs were prepared *via* pyrolysis of ethylenediaminetetraacetic acid disodium salt (EDTA-2Na) at 400 °C under a N_2 atmosphere. They found that when CDs were dispersed in the PVA matrix, phosphorescence was observed upon UV irradiation at room temperature. Comparing the absorption spectra of the CD-PVA composite film and CDs diluted in water, a peak at 220 nm and a broad band centred at 300 nm are observed, which are ascribed to the n–π* transitions of C═O bonds

and π–π* transitions of C=O bonds, respectively. In the phosphorescence spectrum with emission at 500 nm, an excitation band appeared at 260–340 nm which overlapped with the absorption band of the C=O bonds, which indicated that the phosphorescence may originate from the carbon of the C=O bond. Preliminary studies have shown that the phosphorescence of the surface of CDs is derived from the triplet excited state of the aromatic carbonyl group and that the PVA molecules solidify these groups by hydrogen bonding, which effectively prevents energy loss through rotation or vibration.

In addition, through systematic investigations, Li *et al.*[135] reported how the C=N bonds on the surface of CDs affect their RTP performance. Through experiments, it is proved that the C=N bonds are the origin of phosphorescence in this system. They fabricated a RTP CD complex *via* one-pot heat treatment of a mixture of urea and NCDs. Since the dual characteristics of the rigidity of the molten recrystallised urea and the rigidity of the hydrogen bond formed between the biuret and the NCDs make an outstanding contribution to the suppression of the vibrational dissipation of the triplets, the CD system exhibits a longer lifetime than the single-component matrix (Fig. 5a). To determine the effect of hydrogen bonding on the optical properties of HN-powder, they prepared sample 3 (which was secondarily dissolved and dried HN-powder) and sample 4 (which comprised HN-CD solution, urea and biuret in the same ratio as that of sample 3) (Fig. 5b). The result reveals that HN-CDs display the longest lifetime and highest RTP intensity among the three types of CDs, which prove that the triplet relaxation is affected by the hydrogen bonding between HN-CDs and biuret.

Recently, single-component RTP CDs without a matrix have been reported.[130,134] Gao *et al.*[134] presented matrix-free RTP NCDs. The phosphorescence lifetime was 747 ms and the phosphorescence quantum yield (PQY) was 35% when the NCDs were excited by 320 nm UV light. They also found that the phosphorescence intensities and the PQYs increased with the increase in the nitrogen content of the NCDs. They concluded that a high nitrogen content favours the n–π transition, thereby inducing the spin-forbidden transfer of the singlet-to-triplet excited state through intersystem crossing (ISC) to fill the triplet excitons.[136] When the NCDs were dissolved in water, no RTP could be detected. Hydrogen bonds are formed between the internal carboxylic acids of the NCDs which minimised the non-radiative transitions of the triplet excitons. Moreover, the formation of long-chain carboxylic acid dimers on the surface of the NCDs endows the system with oxygen barrier properties, which can hinder the phosphorescence quenching caused by direct collisions between C=O and oxygen molecules. Feng's group reported fluorine, nitrogen co-doped CDs (FNCDs) without a matrix which exhibited RTP properties.[130] A small band

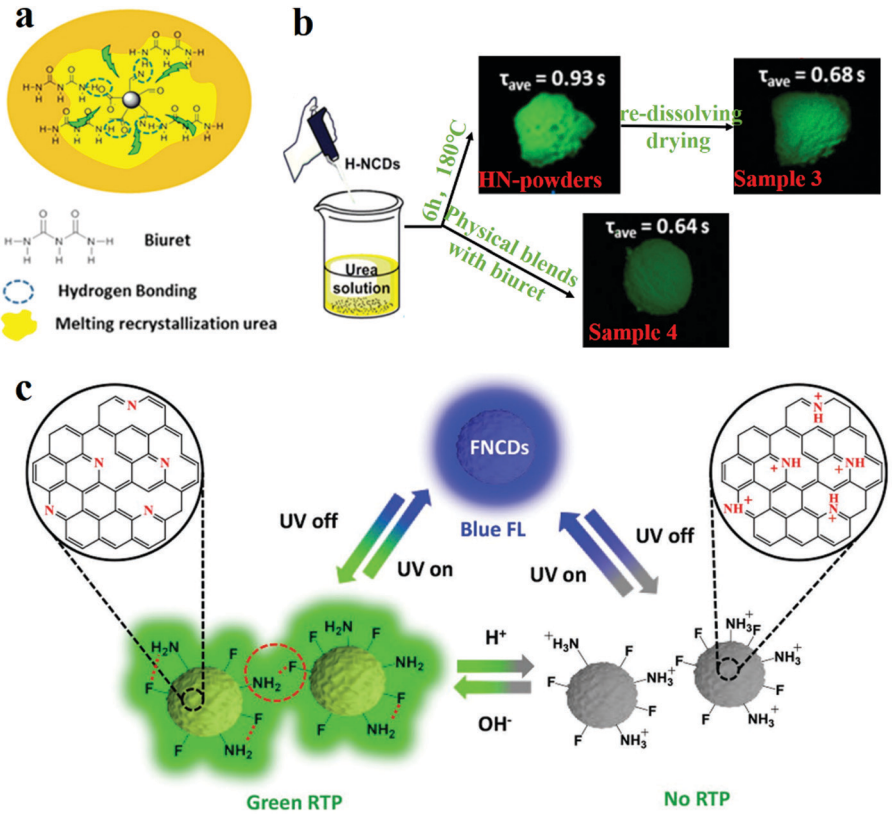

Fig. 5 Schematic of the RTP mechanism and the factors influencing matrix and matrix-free CDs. (a) RTP model of NCDs. (b) Experiments for verification of the influence of hydrogen bonding on phosphorescence lifetime. Reprinted with permission from ref. 135, Copyright 2016, American Chemical Society. (c) Mechanism proposed by Long *et al.* for the pH response of RTP in FNCDs. Reprinted with permission from ref. 130, Copyright 2018, Wiley-VCH Verlag GmbH & Co. KGaA.

gap between the singlet and triplet states of the n–π* electron transitions of C–N/C=N bonds induced self-protective RTP. Further, space protection of the hydrogen and C–F bonds blocked the entry of oxygen, thus reducing the quenching of the RTP. pH-Dependence of RTP was proposed in FNCDs. The hydrogen bonds were formed by deprotonated amino/amide nitrogen and C=N bonds under basic pH conditions, and were beneficial for blocking oxygen and stabilising triplet excitons. However, after the pH is lowered, the hydrogen bond dissociates, and the protonation of C–N/C=N is disturbed, which makes it difficult for ISC to occur between S1 and T1, and the RTP behaviour disappears (Fig. 5c).

2.2.4 Dispersibility and biocompatibility. Dispersibility is a basic property of CDs which is used in industrial production and application; it is mainly related to the surface structure and functional groups of CDs. Several studies show that the hydrophilic and hydrophobic properties of CDs are affected by their preparation methods and the precursors used.[137] Most CDs display good hydrophilicity and dispersibility owing to the formation of oxygen-containing functional groups in the precursor during the synthesis. In addition, mutual transformation between hydrophilicity and hydrophobicity can be realised in CDs by controlling the surface functional groups. For example, Hsu *et al.*[137] reported hydrophilic CDs which were synthesised by a one-pot hydrothermal approach. They proposed that functional groups play a significant role in determining the hydrophilicity of the resulting CDs. Moreover, Mitra *et al.*[138] prepared hydrophobic CDs (HCDs) by microwave pyrolysis of the co-polymer Pluronic F-68 (PF-68); the HCDs were easily dispersed in various organic solvents and revealed a good water resistance.

Low toxicity is a critical property of CDs which is important in bioimaging and medicine. The low toxicity of CDs is mainly owing to their small size, which facilitates their direct removal from biological excretory systems. However, some studies indicated that inhaled nanoparticles can reach the brain and cause degenerative changes to the nervous system.[139] Hence, it is necessary to study the mechanism of toxicity and biocompatibility of CDs. Unfortunately, controlling the toxicity of CDs is not easy because of their complex structure. Therefore, researchers often design non-toxic CDs by selecting a non-toxic precursor as the carbon source of CDs. For example, Sahu *et al.*[140] prepared non-toxic CDs with orange juice as the precursor by one-step synthesis. The CDs were demonstrated to be effective for *in vivo* imaging and as fluorescence probes. In addition, the toxicities of some CDs increased in the presence of external stimuli. Qin *et al.*[141] obtained a type of CD which were prepared by the hydrothermal method by using graphene without any toxicity under nonlight stimulus. However, the CDs were found to be toxic upon irradiation, which is due to light stimulating the production of reactive oxygen species.

3. CDs for optical applications

CDs, as a novel luminescent material, are expected to replace luminescent materials in the optoelectronic field.[23] Based on their fluorescence ability and phosphorescence properties, CDs are gaining increasing attention in optical applications, including data security, chirality, optoelectronic devices, sensing, photocatalysis, *etc.* In this section, these applications of CDs are described.[142]

3.1 CD-based information encryption

Preventing counterfeiting is a worldwide problem, and anti-counterfeiting of high-value items such as legal documents, banknotes, jewellery and fashion items is extremely important.[143] CDs, owing to their responsiveness to stimuli, can generate emission signals of specific wavelengths under external stimulation. The specificity of the response signals endows them with security features, which are difficult to imitate and copy, therefore, they display application potential in the field of ink anti-counterfeiting and data security.[144] Compared to fluorescent organic dyes and rare earth metals, CDs exhibit significant advantages such as high luminescence intensity, good biocompatibility, low toxicity and high chemical and light stability, which indicate that they can replace the traditional luminescent materials in this field in the future.[145]

3.1.1 Fluorescence-based information encryption. Over the past several years, researchers have used CDs as encryption carriers in a large number of data security and anti-counterfeiting studies.[146] For example, Zhu *et al.*[17] synthesised carbogenic CDs. Under excitation with 365 nm UV light, CDs were used as an ink to print invisible patterns, which exhibited sufficiently strong fluorescence. Compared with information hiding and storage by NIR light[147] excitation, UV light excitation offers more advantages such as convenience of carrying and low energy of the UV light source.[146] Liu *et al.*[148] obtained a nitrogen-doped CD (N-CD) ink with a QY of up to 75%, and the information written with this ink was found to be consistent and reproducible under ambient conditions for a long period of time (90 days).

CD-based 1D or 2D codes can effectively prevent tampering or counterfeiting, but, in visible light, they often reveal some imperceptible imprints, which are very disadvantageous for encryption. Hence, it is necessary to develop deeper encryption measures or introduce interference information.[144] Song *et al.*[144] used the chemical oxidation of bulk g-C_3N_4 with HNO_3 and oxalic acid ($H_2C_2O_4$) to prepare invisible CD security inks for printing patterns, wherein the encrypted information is visible only if both the conditions of an appropriate decryption reagent ($NaHCO_3$) and UV light are simultaneously met. The appearance and hiding of fluorescence can be controlled by adding $H_2C_2O_4$ and $NaHCO_3$ solutions, because of the pH dependence of the fluorescence of CDs. In addition, Feng's group[110] reported fluorine-modified CDs (FCDs). They prepared FCDs by solvothermal fluorination, and these were used in solution as printing inks; printed paper treated with the decryption reagent PEG showed a fluorescent pattern under UV light irradiation (Fig. 6b). The results showed that FCDs revealed a longer average fluorescence lifetime (5.31 ns), compared to those of CDs. When FCDs form aggregates with diameters of around 100 nm, fluorescence quenching is caused by the interaction of the hydrogen bonds.

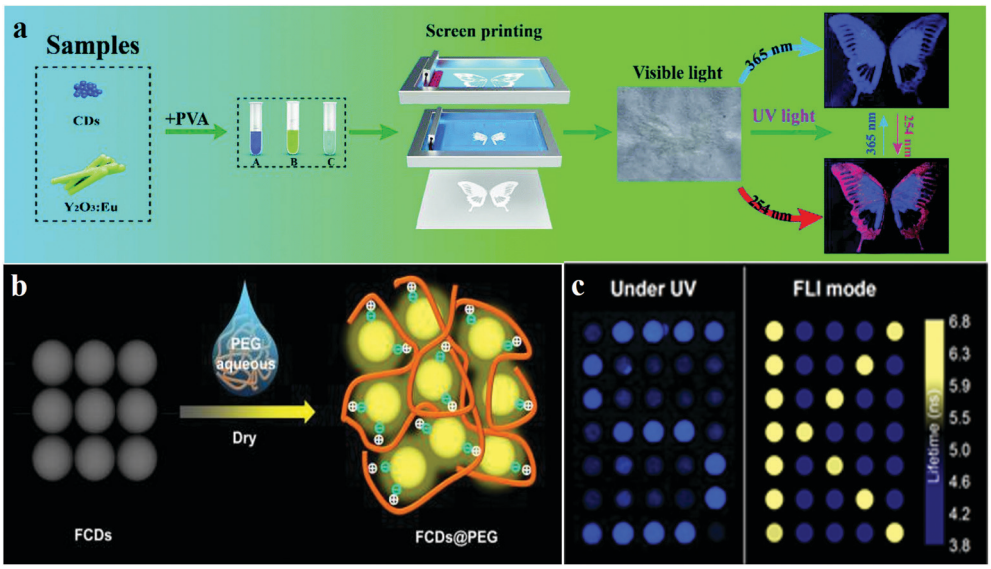

Fig. 6 Schematic of fluorescence anti-counterfeiting mechanism and applications. (a) Li *et al.* reported CDs for anti-counterfeiting application. Reprinted with permission from ref. 146, Copyright 2018, The Royal Society of Chemistry. (b) The addition of PEG affected the fluorescence performance of the FCDs@PEG system. Reprinted with permission from ref. 110, Copyright 2017, American Chemical Society. (c) Kalytchuk *et al.* reported the mechanism of CD fluorescence-lifetime-encoded anti-counterfeiting. Reprinted with permission from ref. 143 Copyright 2018, American Chemical Society.

Moreover, the optical information written on paper by using FCDs can be decrypted and re-encrypted using PEG and water, respectively. For example, ''FCDs'' written using FCD inks exist as aggregates without the addition of PEG, and cannot be observed under UV irradiation, but ''FCDs'' can be observed after treating with PEG. In addition to using decryption reagents as a means of realising multiple encryption systems, a promising approach is to utilise UV light sources of different wavelengths for displaying different information. Li *et al.*[146] demonstrated a new information encryption technique by which two patterns are observed at two wavelengths of light irradiation (namely, 254 and 365 nm UV light). This technique relies on the use of different fluorescent encryption reagents. Three different inks A, B and C were synthesised with pure CDs, pure Y_2O_3:Eu, and a mixture of Y_2O_3:Eu and CDs, respectively. Multi-coloured inks are printed on paper by using screen printing techniques to obtain invisible patterns. The pattern is well-recognised at 254 nm and the information is complete. However, only an incomplete and single blue signal was observed under 365 nm light excitation (Fig. 6a).

In addition to the above anti-counterfeiting methods, Kalytchuk *et al.*[143] reported a conceptual anti-counterfeiting technique with resolution in the nanosecond range by controlling the fluorescence lifetime of CDs. Unique CDs with different fluorescence lifetimes were prepared under different synthesis conditions. Slow fluorescence lifetime (CDs-s) and fast fluorescence lifetime (CDs-f) were obtained under different conditions. Owing to the uniqueness of the fluorescence lifetime of CDs, the images printed with these inks are more difficult to counterfeit and replicate. The fluorescence lifetime of τ_f CDs-f = 7.9 ns and (τ_s) CDs-s = 13.2 ns. A clear resolution of the fluorescence lifetime of CDs makes it possible to encode the anti-counterfeiting information based on the fluorescence lifetime. Then, the lifetime-encoded true symbol ''K'' and the false symbol ''S'' were printed at the same position. The symbol ''S'' can be observed clearly under UV excitation (Fig. 6c, left), but, based on the fluorescence lifetime imaging analysis image, the true signal ''K'' can itself be obtained (Fig. 6c, right). Although this information encryption method is only a concept at present, it may be used in information protection in the future.

3.1.2 Phosphorescence-based information encryption. Conventional anti-counterfeiting technology usually produces monochromatic or multi-coloured fluorescence under the excitation of UV and NIR light. However, with the advancement of materials science, counterfeiting of the traditional anti-counterfeit labels has become easier with replaceable fluorescent materials. Consequently, it is a good suggestion to propose the concept of adding phosphorescence to anti-counterfeiting inks, which can effectively improve the level of security against counterfeiting.[107]

The main components of RTP materials are inorganic or heavy metal complexes. With the progress of CD research, their RTP phenomenon has also been discovered. Initially, researchers fixed CDs in some matrix, such as PVA or $KAl(SO_4)_2{\cdot}x(H_2O)$.[107] For instance, Tian *et al.*[132] prepared CD/PVA composite RTP materials for multi-level data encryption by thermal treatment. For comparison, they synthesised untreated CDs (CD-1) and 200 °C treated CDs (CD-2) and compounded them with PVA. The two films exhibited different phosphorescence temperature dependences. CD-1@PVA showed fluorescence enhancement only at 150 °C, whereas CD-2@PVA exhibited phosphorescence at this temperature. When the temperature rose to 200 °C, CD-1@PVA also displayed phosphorescent properties. As shown in Fig. 7a, the material reveals cryptographic writing performance. CzA@PVA (''CIOMP''), CD-2@PVA (''CD'') and CD-1@PVA (''ots'') are simultaneously edited at the same position when the temperature

is lower than 80 °C under UV illumination, and all three materials exhibit fluorescence; the encrypted information is difficult to distinguish. When the temperature rises to 150 °C, CD-2@PVA shows green phosphorescence, and the first level of encrypted information "CD" appears. When the temperature further increases to 200 °C, the phosphorescence properties of CD-1@PVA and CD-2@PVA are activated, and the second-level encrypted information "ots" also appears.

In addition, Jiang *et al.*[149] prepared ultralong RTP (URTP) nitrogen- and phosphorus-doped CDs by a one-pot method. The URTP CDs reveal a phosphorescence lifetime of around 10 s when observed with the naked eye. To further improve the anti-counterfeiting performance of CD inks by modification, they[150] heated CDs to convert their fluorescence to URTP. They prepared F-CDs which exhibited blue fluorescence by using EDA and phosphoric acid as precursors. As expected, the F-CDs showed a QY of 5.17% in water. The F-CDs were further heat treated at a higher temperature (*e.g.* 280 °C for 2 h, see Fig. 7b). It is worth mentioning that the URTP phenomenon is observed in the heat-treated product (named P-CDs), and its phosphorescence lifetime is up to 10 s when observed with the naked eye. In order to prove the applicability of the materials, they printed the pattern (*e.g.* the label "MOUTAI") directly on a filter paper by using F-CD ink. As shown in Fig. 7b, no information can be found on this paper under daylight, and a blue "MOUTAI" pattern is observed under UV light. Then, a heat gun was used to heat to 300 °C for 30 s, and the green phosphorescence "MOUTAI" pattern was displayed.

Although the above-mentioned studies achieved a variety of anti-counterfeiting systems based on phosphorescent CDs, a universal route to CD-based RTP inks with full colour and long lifetimes still needs to be developed.[151] To overcome these issues, full-coloured URTP was proposed in nitrogen-doped CDs by Xie's group,[151] who used folic acid (FA) and deionised (DI) water, *o*-phenylenediamines and EDA, and ethyl alcohol to synthesise three types of phosphorescent CDs, which were then embedded in urea to obtain three NCD-biuret@urea composites (denoted as NCD1-C, NCD2-C and NCD3-C, respectively). The fluorescence and phosphorescence properties of the CDs were revealed; NCD1-C exhibited blue delayed fluorescence (DF), with a lifetime of 1.11 s at 254 nm excitation, whereas excitation with 365 nm light resulted in green RTP, with a lifetime of 0.53 s. NCD2-C displayed a similar blue FL and green long-life emissions (mainly RTP) upon excitation with 254 or 365 nm radiation. For NCD3-C, the average lifetimes of red RTP (Ex. = 450 nm, Mon. = 625 nm) and yellow DF (Ex. = 365 nm, Mon. = 518 nm) were 0.12 and 0.78 s, respectively. When the three CDs were prepared as anti-counterfeiting inks and printed on paper, the same phenomenon as that revealed by the above results was observed (Fig. 8a). Moreover, FNCDs also exhibited a developing self-protective RTP property.[130] Two kinds of FNCDs were prepared under different pH conditions, and the A and B inks used aqueous alkaline (pH = 12.0) and acidic (pH = 2.0) solutions as dispersants, respectively. As shown in Fig. 8b, ink B does not exhibit RTP performance, and the true information "609" was written using ink A; the pattern was filled with the false information "888" by using B. When UV light is continuously irradiated, the false information "888" is displayed, and the true phosphorescent information "609" is visualised after the UV lamp is turned off. The same principle applies to the appearance and disappearance of leaves. Owing to the phosphorescent nature of self-protecting RTPCDs, FNCDs exhibit inherent advantages in the field of anti-counterfeiting and information security.

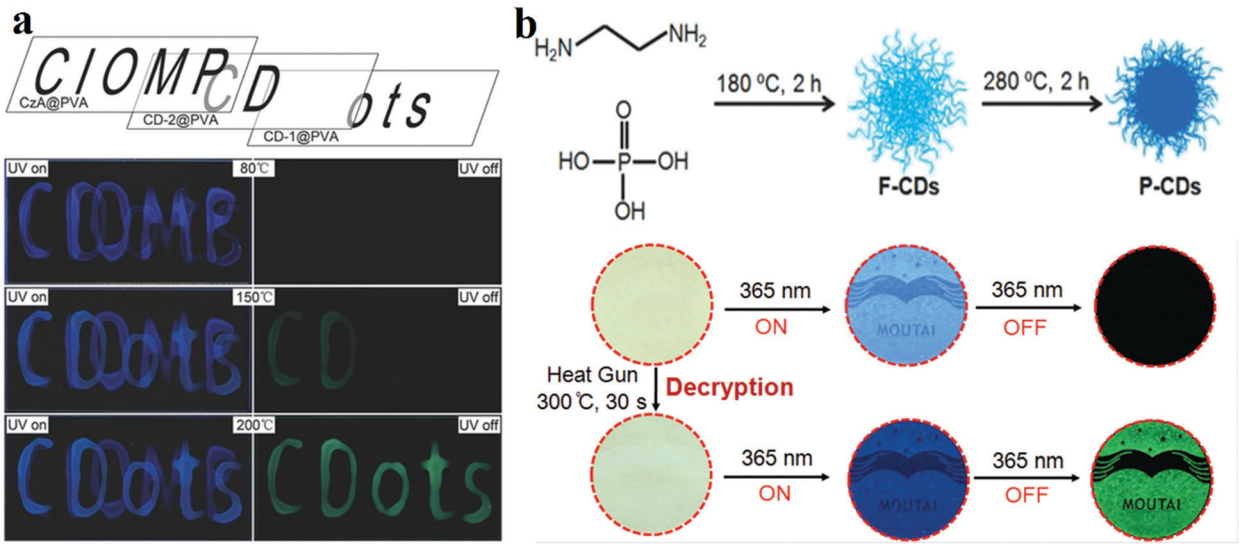

Fig. 7 (a) Schematic diagram of phosphorescence-based multilevel data encryption with a CD/PVA composite under UV light excitation (left) and after switching the UV light off (right). Reprinted with permission from ref. 132, Copyright 2018, Wiley-VCH Verlag GmbH & Co. KGaA. (b) Schematic diagram of the fluorescence-*trans*-URTP of CDs observed upon heating; the top image describes the fabrication of CDs and the conversion of fluorescence to phosphorescence induced by heat treatment, whereas the bottom image presents the application of the CDs. Reprinted with permission from ref. 150, Copyright 2018, Wiley-VCH Verlag GmbH & Co. KGaA.

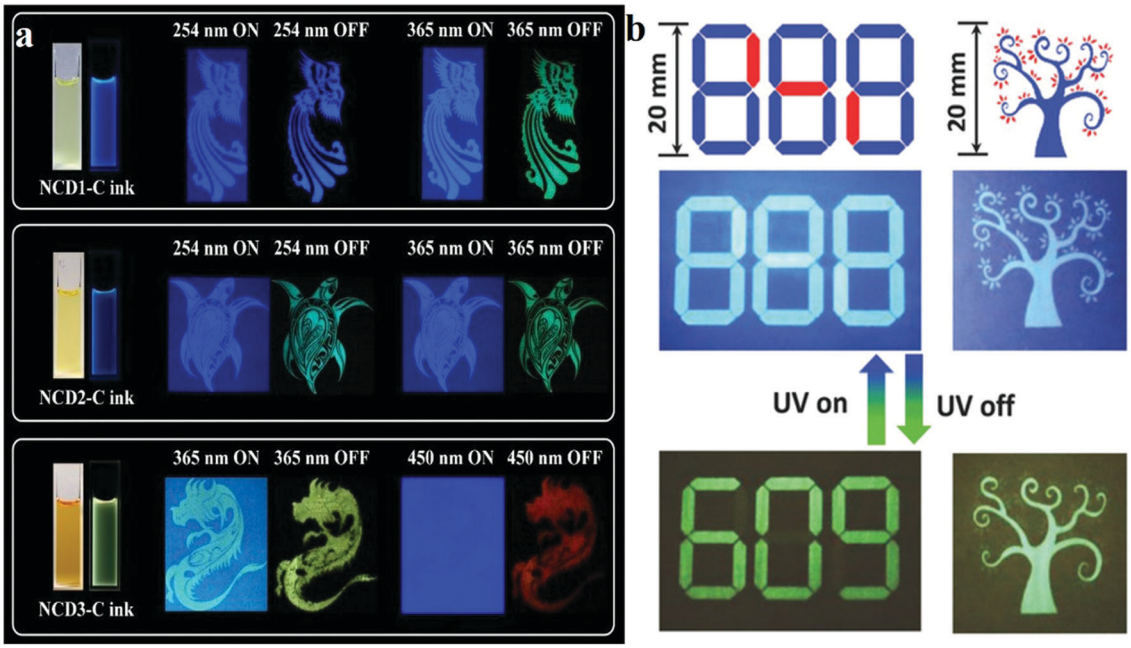

Fig. 8 (a) Schematics of the optical anti-counterfeiting applications of blue, green and red full-coloured RTP nitrogen-doped CDs. Reprinted with permission from ref. 151, Copyright 2019, The Royal Society of Chemistry. (b) Demonstration of lifetime-encoding for security application of self-protective RTP fluorine, nitrogen co-doped CDs. Reprinted with permission from ref. 130, Copyright 2018, Wiley-VCH Verlag GmbH & Co. KGaA.

3.2 CD-based fluorescent sensors

In recent years, through in-depth studies of the fluorescence mechanism of CDs, researchers have found that the enhancement and quenching of the fluorescence of CDs can be regulated by changing the external environment and the binding to chemicals. Thus, CDs can be used as a fluorescent probe to quantitatively detect some parameters. Various sensors based on the fluorescence of CDs have been reported, especially in sensing of ions such as Ag^{+}, Cu^{2+}, Fe^{3+}, Fe^{2+}, and F^{-}, pH sensing and temperature sensing.[45] CDs reveal different fluorescence properties owing to the coordination interaction of the functional groups on the surface, such as hydroxyls (OH^{-}) and carboxyls ($COOH^{-}$), with ions. Wang *et al.*[152] showed hydroxyl functionalised CDs passivated with ethylene glycol; the original CDs were synthesised hydrothermally with glucose. When Fe^{3+} is added to CDs, the hydroxyls present on the surface of the CDs form complexes with Fe^{3+}, and the formed Fe–CD complexes facilitate charge transfer and inhibit exciton recombination, thus decreasing the fluorescence intensity, which leads to significant fluorescence quenching with the increase in Fe^{3+} content (Fig. 9a). In the Stern–Volmer quenching curves, a good linearity between I_0/I and concentration can be observed, which indicates that dynamic quenching processes occur in this sensor system. In addition, Zhu *et al.*[153] integrated a fluorescent nanohybrid sensor for Cu^{2+} based on CDs. This sensor consisted of CDs, CdSe/ZnS QDs and an organic molecule specific to Cu^{2+}, *N*-(2-aminoethyl)-*N*,*N*,*N*′tris(pyridin-2-ylmethyl)ethane-1,2-diamine (AE-TPEA). The CDs, as the blue fluorescence reagent, were synthesised *via* an electrochemical approach. The CdSe/ZnS QDs as the reference signals are inert to Cu^{2+} and display red fluorescence. As shown in Fig. 9b, AE-TPEA functionalised CDs can combine with Cu^{2+} to cause blue fluorescence quenching in CDs, while the red fluorescence of the QDs remains unchanged, therefore, the whole sensor system reveals red fluorescence. Upon the addition of Cu^{2+}, the spectra show that the blue (λ_{em} = 485 nm) fluorescence intensity of the sensor system continuously decreases, whereas the intensity of the red emission (λ_{em} = 644 nm) from the QDs remains constant. For the single CD–TPEA system, its spectrum and photograph reveal blue emission quenching. Compared with the case of the single CD–TPEA system, it is easier to distinguish Cu^{2+} with the naked eye in nanohybrid sensors (Fig. 9c).

Wen and co-workers[154] first proposed a pH sensor based on CDs in 2012. They used CA as the carbon source and 4,7,10-trioxa-1,13-tridecanediamine as the surface coating agent to synthesise nitrogen-doped CDs by thermal pyrolysis. The CDs were then treated with the pH-sensitive fluorescein isothiocyanate and the pH-insensitive Rhodamine B isothiocyanate to yield dual-labelled CDs (DLCDs). Two fluorescence peaks (at 515 and 575 nm upon 488 nm excitation) can be observed for the DLCDs. As the authors indicated, when the pH changed from 4.5 to 9, the intensity of the 575 nm peak only increased slightly, while that of the 515 nm peak increased significantly. To further explore the bio-application of DLCDs, they treated HeLa cells with DLCDs for 24 h and observed that the cell viability was not significantly changed. Then, images of the treated HeLa cell were taken at different pHs and analysed with Olympus software (FV10-ASW) to reveal a characteristic pH-dependent signal (Fig. 10a). In addition, Wu *et al.*[155] obtained nitrogen-doped GQDs *via* the hydrothermal method with CA as the carbon source and dicyandiamide (DCD) as the nitrogen source. The CDs exhibited PL, with a high QY of 36.5%

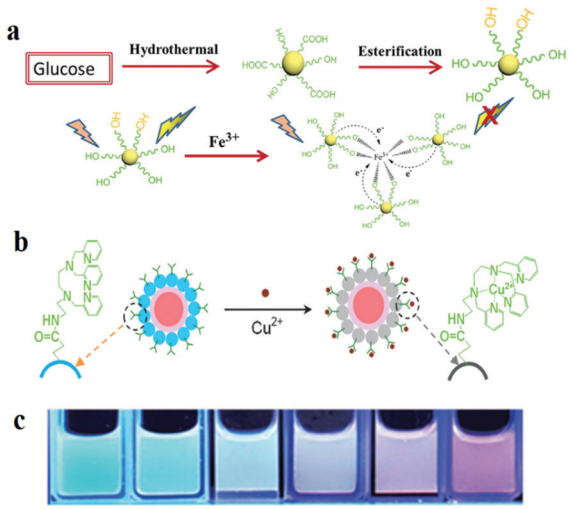

Fig. 9 Schematic of the fabrication and application of two types of CD-based fluorescent ion sensors. (a) Synthesis procedure of the CDs and the formation process of the chelate compound from CDs and Fe^{3+}. Reprinted with permission from ref. 152, Copyright 2017, The Royal Society of Chemistry. (b) Schematic image of fluorescence sensing of Cu^{2+}. (c) CdSe/ZnS CD-TPEA composite ratiometric probe solutions. Reprinted with permission from ref. 153, Copyright 2012, Wiley-VCH Verlag GmbH & Co. KGaA.

and a maximum excitation wavelength of 320 nm at 370 nm. Under 365 nm UV illumination, the PL intensity increased significantly with the change in the pH from 1.81 to 8.95 (Fig. 10b). Then, they added Rhodamine S (RhS) to GQDs. RhS is a fluorescent reagent which is insensitive to pH and appears yellow under 365 nm UV illumination (Fig. 10d). The sensor can estimate the pH based on different coloured (from yellow to pink to purple) fluorescence signals. Furthermore, as illustrated in Fig. 10c, the pH sensor displays good stability when the pH is cycled in the range 2 to 9.

Besides their applications in pH and ion sensing, CDs can also precisely monitor the variation in temperature with the change in fluorescence intensity. Yang *et al.*[156] synthesised nitrogen-doped CDs (N-CDs) by using C_3N_4. Two peaks at 250 and 270 nm are revealed by UV-visible absorption spectroscopy, which are due to the π–π* transition of the aromatic C=C bond. The n–π* transition of the C=O bond induces a low and wide absorption peak at 300 nm which extends to 600 nm. The QY of the N-CDs is 21%, and the PL spectrum displays the highest intensity of emission at 475 nm upon excitation with 400 nm radiation. The results showed that when the temperature is increased from 25 to 80 °C, the PL intensity is reduced by around 46% (Fig. 11b and c). This phenomenon is mainly due to the hydrogen bonds on the surface of the N-CDs formed with water being destroyed at high temperatures (Fig. 11a). In addition, Cui and co-workers[157] reported a temperature-dependent pH sensor based on nitrogen- and sulfur-co-doped CDs. The CDs were prepared *via* a one-pot hydrothermal method with methionine and acrylic acid. TEM revealed an average particle size of 2.3 nm of the CDs; the sizes were within the range 1.5–3.2 nm. The QY of the CDs was also measured as 10.55%. As the temperature increased from 25 to 75 °C, the PL intensity of the CDs decreased linearly, and the fluorescence recovered when the temperature was brought back to 25 °C.

3.3 CD-based light-emitting diodes

In recent years, exploration of electroluminescent diodes (LEDs) has become a hot topic in academic research owing to their applications in liquid crystal displays[158] and illumination devices. At present, researchers are focusing on colloidal semiconductor QDs (sQDs) such as CdSe, CdTe and PbTe, which offer the advantages of high QYs, high emissions, and narrow emission bandwidths. However, as traditional LED raw materials, the disadvantage of QDs which cannot be ignored is their high toxicity to humans and the environment. Therefore, CDs with quantum sizes <10 nm can potentially substitute QDs in LED applications, because of their luminescence characteristics being similar to those of QDs, apart from the advantages of low toxicity and environmental friendliness.[26] Yuan *et al.*[26] reported for the first time bright multi-coloured band gap fluorescent CDs (MCBF-CDs) which were fabricated by using CA and diaminonaphthalene through solvothermal synthesis. The yield of the CDs prepared by this method is about 53%. MCBF-CDs show strong excitonic absorption peaks in the UV-visible absorption spectra which are centred at about 350, 390, 415, 480 and 500 nm for B (blue)-, G (green)-, Y (yellow)-, O (orange)- and R (red)-BF-CDs, respectively. All the five BF-CDs display uniformly and narrowly distributed nanoparticles, the average sizes of which are about 6.68 (R-, QY = 12%), 4.90 (O-, QY = 53%), 3.78 (Y-, QY = 58%), 2.41 (G-, QY = 73%) and 1.95 nm (B-BF-CDs, QY = 75%). MCBF-CD-based monochrome LEDs reveal that L_{max} reaches about 136, 93, 60, 65 and 12 cd m^{-2} in the cases of B-, G-, Y-, O- and R-LEDs, respectively (Fig. 12b). WLEDs have been fabricated by using G-BF-CD-blended poly(9-vinylcarbazole) as an emissive layer. The L_{max} and η_c can be as high as about 2050 cd m^{-2} and 1.1 cd A^{-1}, respectively. The coherent infrared energy (CIE) coordinates of the WLED are (0.30, 0.33), which are quite close to those of pure white light (0.33, 0.33). Subsequently, they also prepared narrow bandwidth emission triangular CDs by threefold symmetric PG, and the multi-coloured LEDs based on NBE-T-CQDs display high colour purities. The L_{max} of B-, G-, Y- and R-LEDs were determined to be about 1882, 4762, 2784 and 2344 cd m^{-2}, respectively, and their η_c reached 1.22, 5.11, 2.31 and 1.73 cd A^{-1}, respectively.[19] Miao *et al.*[159] fabricated a WLED with CDs which is close to pure white light, and its CIE coordinates are (0.33, 0.34). They synthesised multi-coloured CDs through controlled thermal pyrolysis of CA and urea under different reaction conditions. B-, G- and R-LEDs were fabricated using CD/epoxy composites, and the three LEDs demonstrated strong emissions with PLQYs of 38.6%, 29.8% and 7.4%, respectively; the emission peaks were located at ~440, ~540 and ~620 nm, respectively (Fig. 12a).

Although the above products have been able to effectively replace the traditional materials for application in WLEDs, it is essential to develop lighting systems based on high colour rendering index warm light WLED (CRI > 80) for indoor lighting applications. The properties of CDs with a low red

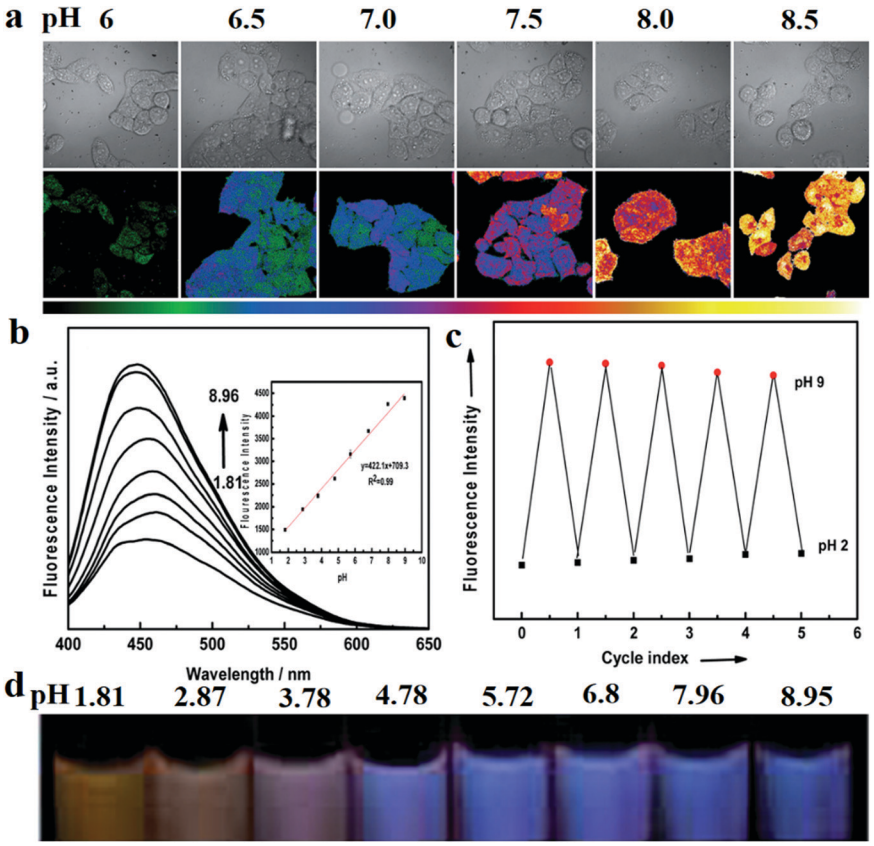

Fig. 10 Images of CD-based fluorescent pH sensor applications. (a) Fluorescence images of HeLa cells marked with CDs at different pHs. The top row shows the differential interference contrast images. The bottom row images (the ratio channel) were generated by software. Reprinted with permission from ref. 154, Copyright 2012, Wiley-VCH Verlag GmbH & Co. KGaA. (b–d) Wu *et al.* reported a pH sensor which was developed with nitrogen-doped GQDs. (b) Fluorescence intensity increases with increasing pH. (c) Cycle stability of the pH sensor. (d) Digital photographs of the pH sensor in different pH buffers under UV illumination. Reprinted with permission from ref. 155, Copyright 2014, The Royal Society of Chemistry.

emission QY limit their use in these applications. Given these challenges, Wang *et al.*[160] fabricated red emitting CDs (R-CDs) with a QY of up to 53% by a sequential dehydrative condensation and dehydrogenative planarization method (Fig. 12d).

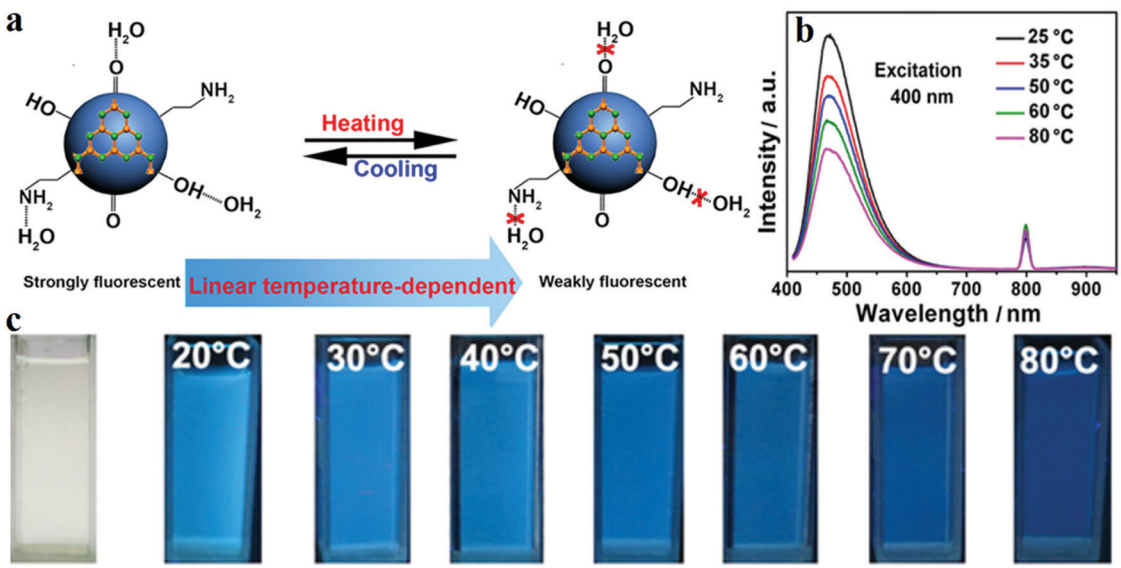

Fig. 11 (a) Schematic diagram of a N-CD temperature sensor. (b) Fluorescence intensity decreases with increasing temperature. (c) Images of the N-CD sensor under UV illumination at different temperatures. Reprinted with permission from ref. 156, Copyright 2015, American Chemical Society.

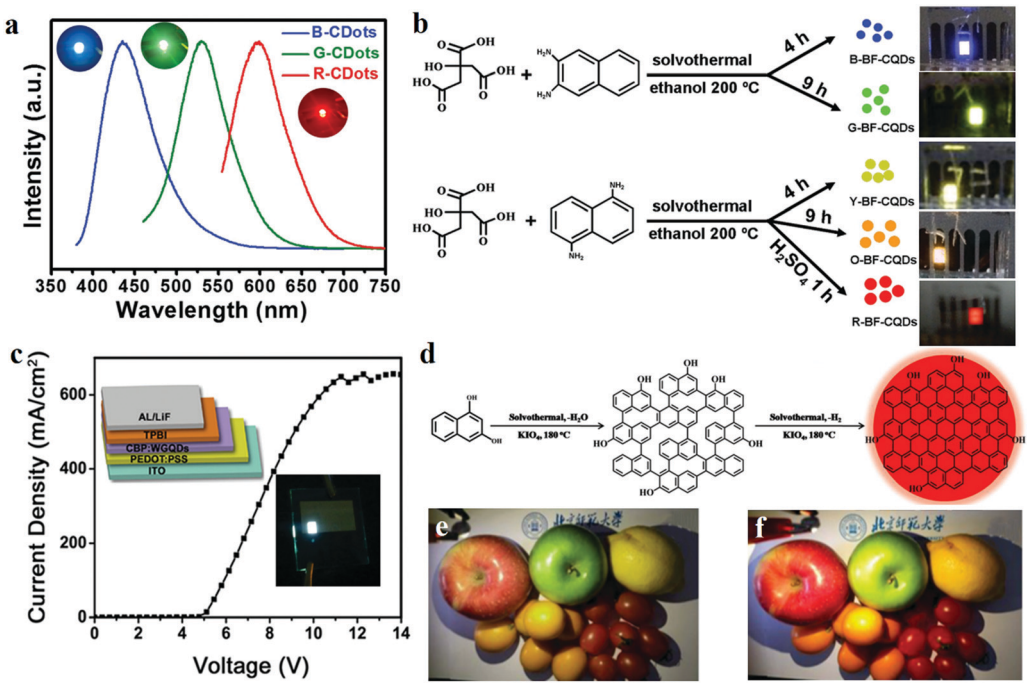

Fig. 12 (a) Optical properties of B-, G- and R-LED devices, as found in Miao's report. Reprinted with permission from ref. 159, Copyright 2018, Wiley-VCH Verlag GmbH & Co. KGaA. (b) Schematics of the preparation of MCBF-CQDs and the application of LEDs. Reprinted with permission from ref. 26, Copyright Wiley-VCH Verlag GmbH & Co. KGaA. (c) Schematic and current density–voltage (*J*–*V*) curve of a WLED based on WGQDs. Reprinted with permission from ref. 162, Copyright 2016, Wiley-VCH Verlag GmbH & Co. KGaA. (d) Schematic of the preparation of R-CDs. (e and f) Photographs of (e) a commercial WLED lamp and (f) a CQD warm WLED lamp. Reprinted with permission from ref. 160, Copyright 2017, Wiley-VCH Verlag GmbH & Co. KGaA.

They demonstrated a WLED based on R-CDs, B-CDs and G-CDs. The correlated colour temperature (CCT) of the WLEDs showed the CIE colour coordinates of (0.4048, 0.3850), which reached that of warm white light (3465 K). Compared with that of the standard warm light (CIE 1931; CCT of 3875 K, which corresponded to CIE coordinates of (0.3924, 0.3912)), the CRI of this warm WLED reached 97 (Fig. 12e and f). Compared with commercial WLED lamps (CRI $\approx$ 82), the CD-based WLED lamps display the true colours of fruits more perfectly. In addition, Yang's group[161] reported novel PCDs which were prepared by hydrothermal treatment of dopamine and *o*-phenylenediamine. The PCDs revealed NIR-emission performance (centred at 710 nm, PLQY of 26.28%). A red LED was fabricated based on the PCDs, and the spectra of the NIR-PCNDs in the LED devices showed an emission with the CIE colour coordinates of (0.67, 0.33).

Apart from the method of synthesis of multi-coloured CDs for WLEDs, Luo *et al.*[162] prepared CDs through a microwave-assisted hydrothermal method with graphite. The CDs directly revealed a novel white fluorescence performance. Two emission peaks appeared in the spectrum of the CDs when they were excited by UV light: a broad band at 445 nm and a weak peak at 575 nm. The researchers also fabricated a WLED in which the CDs acted as single-phase white-light-emitting phosphors. The current density–voltage (*J*–*V*) curve of the WLED shows that the turn-on voltage is about 5 V (Fig. 12c), and the current density increases with the increase in the voltage up to 10 V; then, the current density is stable at around 650 mA cm^{-2} in the range 11–14 V. The CIE coordinates of the WLED are (0.24, 0.25), (0.25, 0.27), (0.26, 0.28) and (0.27, 0.29) for the applied voltages of 11, 12, 13 and 14 V, respectively. Fig. 13 showed some reported CIE colour coordinates of the LED lamp.

3.4 Emerging chiral CDs

Natural processes provide many examples where chiral compounds[163–165] such as chiral molecules[166–168] and chiral liquid crystal materials[43,169–172] are synthesised. As a property of materials, chirality has attracted the attention of researchers for many practical applications such as chiral drug recognition, chiral molecular biology, chiral molecular biology and optical applications. With the development of modern spectroscopy, the optical characteristics attributable to chirality have been studied more deeply, including circularly polarised luminescence (CPL) and electronic circular dichroism (ECD or, in short, CD).[173] The research on chiral CDs started late, but has been developing rapidly. Chiral CDs was first proposed by Vazquez-Nakagawa *et al.*[163] They demonstrated the method of preparing GQDs by exfoliating and oxidatively cutting graphite in a mixture of H_2SO_4 and HNO_3 of high concentrations. They showed that the chirality of GQDs can be easily transferred to supramolecular assemblies composed of small molecules such as pyrene. Then, Suzuki *et al.*[174] used a similar method to synthesise GQDs. To prepare chiral GQDs, the amine group of chiral L-(or D-) cysteine was linked to the carboxyl group of GQDs by the carbodiimide/*N*-hydroxysuccinimide (EDC/NHS) crosslinking method (Fig. 14a). Both the L- and D-forms of CDs exhibit strong emissions at 520–550 nm when excited by UV

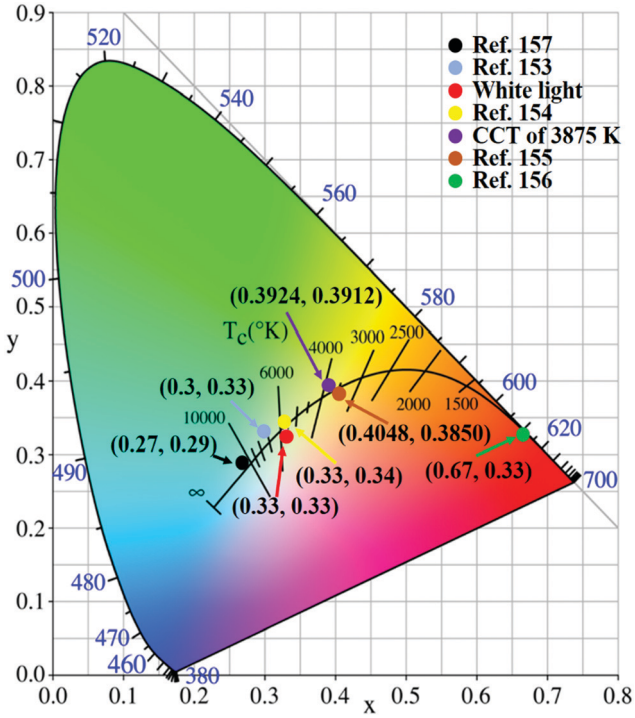

Fig. 13 The reported CIE colour coordinates of the LED lamp.

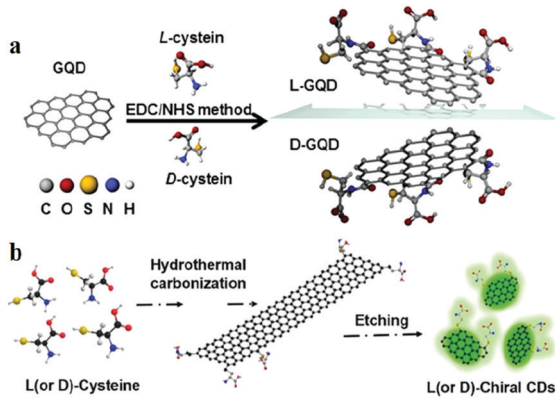

Fig. 14 (a) Molecular schematics of chiral GQD synthesis by the EDC/NHS method. Reprinted with permission from ref. 174, Copyright 2016, American Chemical Society. (b) Synthesis of chiral CDs by hydrothermal treatment of chiral cysteines. Reprinted with permission from ref. 175, Copyright 2018, Wiley-VCH Verlag GmbH & Co. KGaA.

light (λ_{ex} = 330 nm). Nevertheless, the emission peaks of GQDs display a slight red shift after amino acid modification. Raman spectroscopy revealed that the original and chiral GQDs display the same A_{1g} D band (at 1355 cm^{-1}) and E_{2g} G band (at 1590 cm^{-1}). This indicated that the integrity of the centre of the graphene sheets was not destroyed by the surface modification of cysteine. In addition, Li *et al.*[175] used L- and D-cysteine to synthesise chiral L-CDs and D-CDs by hydrothermal treatment at 60 °C; then, the pH of the solution was adjusted to ~8–9 with 0.5 M NaOH for etching (Fig. 14b). The PQY of the L-CDs reached 41.26%, and the average lifetime (Ex. = 405 nm, Mon. = 510 nm) of the dominant component was 7.56 ns. Through UV-visible spectroscopy, it was observed that L-CDs display a weak absorption peak at 400 nm and two distinct absorption peaks at 243 and 300 nm. The π–π* transitions of the aromatic sp^2 domains induced the formation of the peak at 243 nm, whereas the peak at 300 nm may be due to the n–π* (carboxyl and/or C–N/or C–S) transitions. L-CDs and D-CDs produce mirrored spectral images after circular dichroism scanning. Moreover, Zhang *et al.*[176] synthesised chiral CDs by using L- and D-cysteine and CA. This strategy involves directly transferring the chiralities of L- and D-cysteine to CDs through one-pot facile hydrothermal treatment, and the chiral CDs can be enantioselectively recognised by electrochemical analysis. The mirror image CD spectra reveal that L-CDs and D-CDs are enantiomers. More specifically, the chirality was judged based on the electrochemical properties of L-CDs and D-CDs, which were measured using linear sweep voltammetry and electrochemical impedance spectroscopy. For L-CDs, owing to the significant redox reaction between L-CDs and L-tart, the semicircle in the high-frequency region for L-tart is smaller than that for D-tart. D-Tart exhibits a lower onset potential (~1.0 V *vs.* the reversible hydrogen electrode) and a higher ability to oxidise D-CDs.

Using bottom-up microwave-assisted hydrothermal synthesis, Đorđević *et al.*[18] fabricated chiral CDs-R and CDs-S by using arginine and (*R*,*R*)- or (*S*,*S*)-1,2-cyclohexanediamine (CHDA) as the core precursors, respectively. The chiral CDs with sizes below 10 nm displayed two UV-visible absorption peaks at around 270 and 330 nm in the spectra of CDs-S and CDs-R, which are due to the π–π* and n–π* electron transitions of C=O and C=C. It can be seen from the ECD spectrum that the chirality of (*R*,*R*)- or (*S*,*S*)-CHDA was confirmed for the CDs. In addition, the fluorescence of the two CD enantiomers was detected by measuring the opposite circular dichroism signals. The opposite signals confirm the existence of opposite chiral signals in the ECD spectrum. Unfortunately, no chiroptical CPL signal was detected in the excited state, which indicated that there is no chiral information corresponding to the excited state of CDs. Then, the chirality of CDs was investigated by vibration circular spectroscopy (VCD) and density functional theory (DFT) calculations. The VCD patterns of aqueous CNDs-S and CNDs-R solutions show a mirror image relationship with strong bands centred at around 1350 and 1600 cm^{-1}, respectively. The DFT calculations revealed a similar result. Comparison of the VCD patterns and the results of DFT calculations proved that the chirality originates from the CHDA groups located on the surface of the CDs.

In addition to modifying the surface of CDs to obtain chiral CDs from chiral molecules, two oppositely chiral CDs can be fabricated with an L- or D-enantiomer as the only carbon precursor.[177,178] Arad *et al.*[177] reported chiral CDs which were fabricated from either L-lysine (Lys) or D-Lys enantiomer by hydrothermal treatment. TEM reveals a diameter of 4 ± 1.2 nm of the CDs, and the ECD spectrum of Lys-CDs exhibits mirror image ellipticity. Ghosh *et al.*[178] also directly synthesised chiral CDs from the chiral precursor guanosine 5′-monophosphate. When the excitation wavelength increased from 310 to 420 nm, the PL peak of the CDs changed from 447 to 462 nm. Further, the CD spectrum showed several chiral peaks, including negative

peaks at 230 and 260 nm, intense positive peaks at 218 and 270 nm and a shoulder peak at 300 nm. Newly developed chiral CDs have been found to have an effect on the growth of living organisms. For example, Zhang *et al.*[179] reported the hydrothermal method of synthesising chiral CDs by using CA and cysteine as precursors. It was found that the chirality of CDs had an effect on plant growth (mung bean was the model plant in this study). When the content of the chiral CDs was less than 500 μg mL^{-1}, the growth rate of mung bean sprouts increased with the increase in the CDs. A series of experiments have shown that chiral CDs both facilitate the growth rate by promoting the photosynthesis of plants and improve the performance of D-CDs.

4. CDs for energy applications

With the development of science and technology, the global energy consumption continues to grow. Therefore, development of clean, efficient and affordable renewable energy is increasingly urgent.[24,180] As a newly developing material, CDs display wide application prospects in the field of energy, and may reduce the costs of solar cells, supercapacitors and lithium-ion batteries (LIBs) and can even greatly improve their performances.[23]

4.1 CD-based catalysts

With the rapid development of the economy and industry, the global energy crisis and environmental issues have become the most pressing challenges. In this context, the selection of suitable electrochemical catalysts is helpful to improve energy efficiency. The cathodic oxygen reduction reaction (ORR) is one of the most crucial factors affecting the performance of a fuel cell. However, current Pt catalysts are expensive and commercially unavailable. Choosing CDs as the electrocatalyst is helpful to realize the large-scale application of fuel cells.

Qiu's group reported an all-carbon hybrid electrocatalyst using nitrogen-doped CDs decorated on graphene (NCDs/G). They compared with electrocatalytic performances of NCDs/G and Pt/carbon black (Pt/C) electrode by cyclic voltammetry in an O_2-saturated 0.1 M KOH solution, N-CDs/G electrode changes are not obvious, but a strong response for the commercial Pt/C catalyst is detected. This novel electrocatalyst demonstrated comparable electrocatalytic activity, and better durability and methanol tolerance than those of the commercial Pt-based electrocatalysts for the ORR.[181] Besides, Qu's group also fabricated nitrogen-doped CD electrodes with willow leaves. In CVs for O_2 reduction measurements, a characteristic ORR peak appeared at *ca.* −0.22 V in the O_2 saturated solution, indicating the effective electrochemical reduction of oxygen initiated on this electrode.[182]

On the other hand, solar energy, as a form of clean renewable energy which is inexhaustible, plays a critical role globally. At present, photocatalysis has become one of the most eye-catching applications of solar energy. On one hand, CDs reveal a wide light absorption range, from deep UV to NIR. On the other hand, CDs can be used as an excellent electron donor and acceptor, and their electron transport capability is attributed to fluorescence resonance energy transfer (FRET). Hence, CDs have an important research value as a new generation of photocatalytic materials.[109,183] Based on the application type, CD-derived photocatalysts can be classified into four types, as those for photocatalytic degradation, CO_2 conversion, solar water splitting and chemical reactions.

The pollution of the atmosphere and the water environment has become a huge obstacle to the sustained and steady development of mankind. CDs can be used in the degradation of pollutants as a component of photocatalysts. Wang *et al.*[184] synthesised CD carbocatalysts by the hydrothermal method with glucose and HCl. The PLQY of the CD-based carbocatalysts reached 9.1%, and the PL spectra of the CD-based carbocatalysts showed UCPL properties (long excitation wavelengths, ranging from λ_{ex} = 700 nm to λ_{ex} = 980 nm, and emissions ranging from 454 to 544 nm). The CD carbocatalysts were also capable of catalytically reducing 4-nitrophenol (Fig. 15a). Under NIR irradiation, almost all 4-nitrophenol molecules can be reduced within 8 min in the presence of the CD-based carbocatalyst at a power density of 1.5 W cm^{-2}. When only the light source was changed to visible radiation, under the same conditions, the amount of 4-nitrophenol reduced was 59.5%. After 5 runs, the performance of the CD-based carbocatalyst in the degradation of 4-nitrophenol reached 92.7%. In addition, CDs are also capable of photocatalytically degrading Rhodamine B and methylene blue (MB). Aghamali and co-workers[185] reported CDs which were fabricated *via* hydrothermal carbonisation by using diethylenetriamine as a nitrogenous surface passivation reagent and CA as the carbon source. The CDs exhibited extensive light absorption properties, including sunlight and visible light absorption. As photocatalysts, CDs display UCPL and can utilise visible light of longer wavelengths (600–790 nm) to display PL at a shorter wavelength (431 nm). Thus, CDs can effectively photocatalyse the degradation of MB. For the same period (160 min), in the presence of sunlight, the removal rate is 23% more than when the sample is exposed to visible light. Besides, CDs can play an additional role in improving the photocatalytic degradation yield. For example, a CDs/Ag/Ag_3PO_4 complex photocatalyst reveals better performance, compared with other catalysts such as Ag_3PO_4 and Ag/Ag_3PO_4 (Fig. 15b). And only the CDs/Ag/Ag_3PO_4 catalyst can make the colour of methyl orange (MO) almost disappear within 10 min. It demonstrated that the order of photocatalytic abilities of Ag_3PO_4 and related complex photocatalysts is CDs/Ag/Ag_3PO_4 > CDs/Ag_3PO_4 > Ag_3PO_4 > Ag/Ag_3PO_4. Furthermore, light irradiation is crucial for the degradation process.[186] Ke *et al.*[187] enhanced the photocatalytic performance of TiO_2 by doping CDs. MB was the target pollutant, and the degradation efficiency of the CDs–TiO_2 complex is significantly higher than that of controlled pure TiO_2. When the volume of CDs used is 10 mL, the degradation efficiency is the highest, up to 90%, which is 3.6 times as high as that of pure TiO_2. With the increase in the amount of CDs added from 5 to 10 mL, the catalytic activity of CDs–TiO_2 increased rapidly due to enhanced visible light absorbance and improved separation efficiency of the photogenerated charge carriers.

In addition to the degradation of pollutants, photocatalytic water splitting for hydrogen production and CO_2 conversion is an effective measure to address the global challenges in the

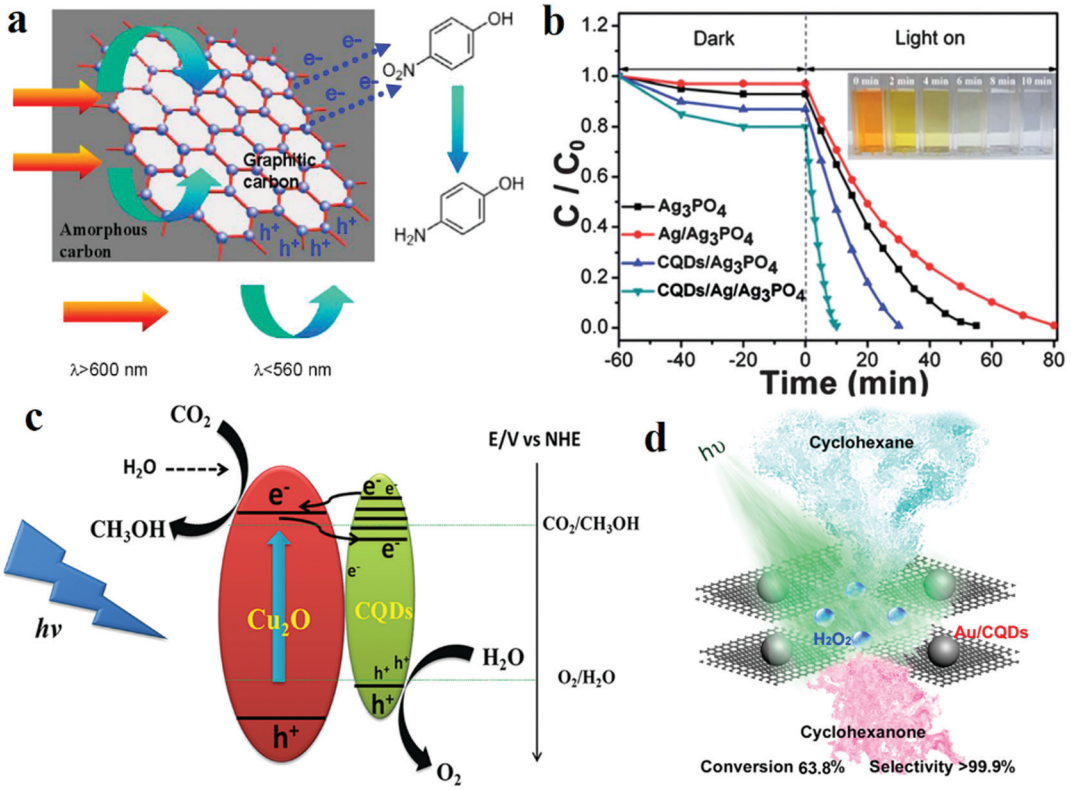

Fig. 15 Schematic of CD-based photocatalysts: photocatalytic degradation, CO_2 conversion and chemical reactions. (a) Diagram of the photocatalytic reduction of 4-nitrophenol to 4-aminophenol over CD-based carbocatalysts. Reprinted with permission from ref. 184, Copyright 2015, American Chemical Society. (b) Photocatalytic activities for MO degradation. Reprinted with permission from ref. 185, Copyright 2018, Elsevier B.V. (c) Diagram of the photocatalytic CO_2 reduction by CDs/Cu_2O. Reprinted with permission from ref. 192, Copyright 2015, Wiley-VCH Verlag GmbH & Co. KGaA. (d) Diagram of the selective oxidation of cyclohexane by using the Au/CDs composite as a photocatalyst. Reprinted with permission from ref. 193, Copyright 2013, American Chemical Society.

production of clean, inexpensive renewable energy and greenhouse gas absorption. More specifically, the overall water splitting reaction consists of two half-reactions. One is the H_2-evolution reaction (HER) and the other is the O_2-evolution reaction (OER). The typical four-electron reaction equations are the following.

$$2H_2O(l) \rightarrow O_2(g) + 2H_2(g) \quad (1)$$

$$H_2 \text{ generating site: } 4H^+ + 4e^- \rightarrow 2H_2(g) \quad (2)$$

$$O_2 \text{ generating site: } 2H_2O(l) \rightarrow O_2(g) + 4H^+ + 4e^- \ 1.23 \text{ eV} \quad (3)$$

Two-step pathway to products H_2 and O_2. First, H_2 and H_2O_2 are generated from water:

$$2H_2O(l) \rightarrow H_2O_2(l) + H_2(g) \quad (4)$$

$$H_2 \text{ generating site: } 2H^+ + 2e^- \rightarrow H_2(g) \quad (5)$$

$$H_2O_2 \text{ generating site: } 2H_2O(l) \rightarrow H_2O_2(l) + 2H^+ + 2e^- \ 1.78 \text{ eV} \quad (6)$$

Second, disproportionation of H_2O_2 releases energy:

$$H_2O_2(l) \rightarrow 1/2O_2(g) + H_2O(l) \ \Delta G = -106.1 \text{ kJ mol}^{-1} -1.1 \text{ eV} \quad (7)$$

Upon irradiation with light of a suitable wavelength, electrons are excited onto the conduction band and leave holes on the valence band. The e/h^+ pairs are then transferred to the photocatalyst surface to initiate the HER and OER, respectively.[109]

Yeh *et al.*[188] reported the use of nitrogen-doped graphene oxide-quantum dots (NGO-QDs) as a photocatalyst. Both p- and n-type conductivities are observed in NGO-QDs. The p-type conductivity is due to the formation of an enriched layer at the graphene oxide/water interface, which is beneficial for the reduction of water to hydrogen. In addition, the n-type characteristic of the nitrogen-containing graphene oxide promotes the migration of holes for the oxidation of water to oxygen. Through experimental analysis, pure water was decomposed by the NGO-QDs catalyst under external visible light irradiation (420 nm $< \lambda <$ 800 nm). The products (H_2 and O_2) were steadily produced from the system at the $H_2:O_2$ ratio of around 2 : 1. No N_2 evolution was observed in this system. A comparison shows that the water-splitting activity of NGO-QDs is about half that of $Rh_{2-y}Cr_yO_3$/GaN:ZnO. Kang's group[189] fabricated a metal-free CDs–carbon nitride (C_3N_4) nanocomposite photocatalyst. The QY of the CDs reached 16% at $\lambda = 420 \pm 20$ nm, 4.42% at $\lambda = 600 \pm 10$ nm and 6.29% at $\lambda = 580 \pm 15$ nm. The overall solar energy conversion efficiency of the system was 2.0%. They also demonstrated the evolution of H_2 and O_2 from aqueous CDs–C_3N_4 composite solution under visible light irradiation. The collected gas revealed a molar ratio of H_2 to O_2 of 2.02 and no other gas (*e.g.*, CO_2 or N_2). The H_2 generation

rate under the standard conditions increased by a factor of 5.4 for CDs–C_3N_4 containing a higher concentration of CDs. Zhang *et al.*[190] used a homogeneous "spot heating" approach to fabricate a type of photocatalyst. The photocatalysts are composed of highly crystalline CDs and 2D C_3N_4 nanosheets. The addition of CDs extended the light absorption spectrum, and reduced the effective mass of electrons (e^-), facilitating photocarrier transport from the excited sites. The CDs/C_3N_4 catalyst has a H_2 production rate (152 μmol g^{-1} h^{-1}) that is several times higher than that of pure C_3N_4.

As far as CO_2 conversion is concerned, Cao *et al.*[191] reported an approach involving the use of surface-functionalised CDs to harvest visible photons capable of surface charge separation for driving the photocatalytic reduction of CO_2. By using a CD photocatalyst for the reduction to only formic acid, the QY of the photocatalytic reactions of CO_2 was ~0.3%. Under the same experimental conditions, the QY of the traditional photocatalyst containing suspended TiO_2 nanoparticles was reduced by an order of magnitude (again for only formic acid formation). Moreover, utilising the synergistic effect of CDs with other photocatalysts, CDs can dramatically increase the photocatalytic efficiency of CO_2 conversion. For example, Li *et al.*[192] reported a CDs/Cu_2O composite heterostructure photocatalyst for solar-light-driven conversion of CO_2 to methanol (MeOH). CO_2 and MeOH were photoreduced by the CDs/Cu_2O composite at the rate of 56 μmol g^{-1} h^{-1}, which is much higher than the reaction rate previously obtained when using Cu_2O or Cu_2O-based materials as catalysts (38 mol g^{-1} h^{-1}). The high catalytic activity is due to CDs acting as a photogenerated hole-acceptor. Mechanistically, the electron consumed in the reduction of CO_2 to MeOH is produced by visible light excitation of the surface of Cu_2O. On the other hand, holes oxidise H_2O to O_2 on the surface of the CDs (Fig. 15c).

The preparation of highly efficient, highly selective catalysts is currently the main goal in catalytic chemistry and chemical production. Although the development of new catalysts for cyclohexane oxidation has made great progress, the current industrial production processes still suffer from problems such as low conversion rates, excess production of wastes and poor selectivities. Liu and co-workers[193] demonstrated CD-based photocatalyst systems for green oxidation of cyclohexane. Cyclohexane was subjected to green oxidation to cyclohexanone with H_2O_2 under visible light irradiation at room temperature by using an Au nanoparticle/CDs composite photocatalyst; the conversion was 63.8%, and the selectivity was 99.9% (Fig. 15d).

4.2 CD-based solar photovoltaics

With over 86 PW of its energy reaching the earth's surface every year, the sun is a key player in the paradigm shift from our unsustainable and environment-polluting petroleum-based economy. Unfortunately, harnessing this solar energy *via* photovoltaic processes is currently hindered by the high cost-to-energy output ratios, which necessitates the development of low cost, higher efficiency devices. In addition, many state-of-the-art devices are based on unsustainable and environmentally hazardous materials, which will require greener replacements for a solar-energy-based economy to be realised.[194] CDs are more popular, versatile materials for these devices owing to their unique optical and eco-friendly properties, which are comparable with those of well-known sQDs.[25] Because of the photophysical properties of CDs, they can be applied in dye sensitised solar cells (DSSCs) as a light-harvesting dopant. Dou *et al.*[195] obtained CDs *via* the hydrothermal method with red algae. The obtained CDs exhibited good water solubility, a QY of 3.12% and an average size of 4.87 nm. CDs can be used as a light harvester in mesoscopic solar cells. The maximum power conversion efficiency of a solar cell customised with CDs/N719 is about 1% higher than that of a system without CDs. As shown in Fig. 16a, the HOMO and LUMO levels of the synthesised CDs are −5.4 and −4.1 eV, respectively. The HOMO edge of CDs (−5.4 eV) matches that of the N719 dye (−5.45 eV) and the redox potential of the I^-/I_3^- dipole (−4.9 eV), which indicates extraction of pores from N719 to the electrolyte. The bridge helps achieve efficient electron–hole separation and improved voltage output. Moreover, the narrow band gap (1.2 eV) of CDs makes it possible to absorb NIR light below 1097 nm and excite electrons to the conduction band of TiO_2. In addition, Briscoe *et al.*[196] synthesised three different types of CDs as sensitisers for ZnO-nanorod-based solid-state nanostructured solar cells. These CDs were prepared by simple one-step hydrothermal carbonisation of glucose (G), chitin (CT), and chitosan (CS). The fluorescent QY of the aqueous CQD solution was calculated to be 11.6% for CT-CDs, 13.4% for CS-CDs and 1.4% for G-CDs. ZnO was soaked in the CD solutions for 24 h, then, three CDs were coated on the surface of ZnO. The highest efficiency of 0.077% was observed for the devices produced through the combination of CS- and CT-CDs. Although these CDs and devices can be produced highly inexpensively by simply using solution methods, the efficiency still needs to be improved before this process can enter the market as a mature technology.

Further, CDs show prospects for application as an electron transporting material in bulk-heterojunction solar cells. Kang *et al.*[197] revealed that CDs can be applied as a tunnel junction (TJ) intermediate connection layer (ICL). They added CDs to the PEI layer as a dopant. Thereby, the electron extraction performance of the single-junction solar cell is improved, and the tandem solar cell displays a better series connection. Fig. 16b presents a schematic illustration of a single-junction solar cell structure. The single-junction solar cell with a pristine PEI layer yields a fill factor (FF) of 0.673, with a V_{OC} of 0.774 V, a J_{SC} of 16.430 mA cm^{-2} and a PCE of 8.56%. When the doping level is increased (up to 0.5%), the solar cell performance improves. However, when the doping level exceeds 5%, the efficiency is reduced. Compared with that of PEI ICL, the EQE of the CD-doped PEI ICL increases with the increase in the doping level up to 0.5%, but when the doping level increases up to 1.0% from 0.5%, the EQE decreases. In addition, Choi *et al.*[198] reported highly efficient perovskite solar cells based on surface plasmon resonance (SPR)[199] enhancement with CD-supported silver nanoparticles. The SPR effect of CDs–Ag nanoparticles significantly improves the radial emission and permits additional

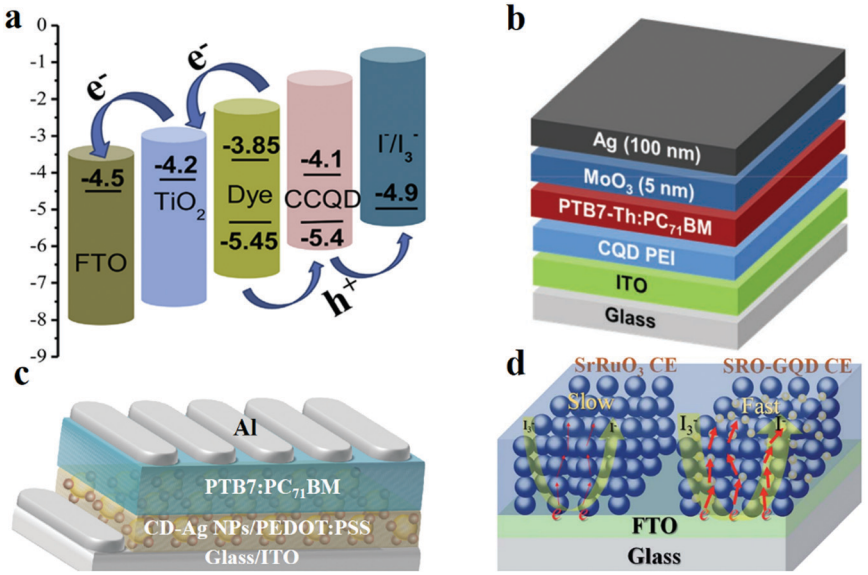

Fig. 16 (a) The energy level distribution and charge transfer within the photoanode. Reprinted with permission from ref. 195, Copyright 2018, Elsevier B.V. KGaA. (b) Schematic illustration of the single-junction solar cell structure. Reprinted with permission from ref. 197, Copyright 2018, Wiley-VCH Verlag GmbH & Co. KGaA. (c) Device structure of a polymer solar cell with CDs–Ag nanoparticles. Reprinted with permission from ref. 198, Copyright 2013, Springer Nature. (d) The schematic diagram of the reduction reaction of $SrRuO_3$ and SRO-GQD CE. Reprinted with permission from ref. 200, Copyright 2017, The Royal Society of Chemistry.

light absorption. The device structure employed was glass/ITO/CDs–Ag nanoparticles/PEDOT:PSS/PTB7:PC71BM/Al (Fig. 16c). The device with CDs–Ag nanoparticles displays a V_{OC} of 0.75 V, a J_{SC} of 16.0 mA cm^{-2}, a PCE of 8.31% and a FF of 0.70. These values are higher than those of a device without the CDs–Ag nanoparticles (J_{SC} of 14.4 mA cm^{-2}, V_{OC} of 0.75 V, FF of 0.70 and PCE of 7.53%).

The dye regeneration reaction in DSSCs involves the catalytic reduction of triiodide (I^{3-}) to iodide (I^-), wherein the electrons required for the reduction reaction are collected from an external circuit by the CE. Platinum is the most widespread choice for CEs. However, its poor stability and high cost have limited the large-scale production and commercial application of DSSCs. Electrically conductive perovskites (general formula ABO_3, *e.g.* $SrRuO_3$) may be a good choice for the DSSC CE. CDs can modify perovskites to enhance their electronic performances. For example, Liu *et al.*[200] fabricated a CD-decorated $SrRuO_3$ mesoporous film as an efficient CE. Specifically, the CDs were synthesised by a facile hydrothermal technique with CA and thiourea. The speed of catalysis of the reduction of I^{3-} to I^- is higher for SRO-GQD hybrid CEs than for $SrRuO_3$ CE (Fig. 16d). Under one sun illumination (AM 1.5G, 100 mW cm^{-2}), the photovoltaic parameters of the DSSCs assembled with different CEs are as follows. The $SrRuO_3$ CE exhibits a J_{SC} of 14.99 mA cm^{-2}, a V_{OC} of 771 mV and a FF of 0.62, which result in a PCE of 7.16%. The SRO-GQD CE exhibits a J_{SC} of 15.62 mA cm^{-2}, a V_{OC} of 758 mV and a FF of 0.68, which result in a PCE of 8.05%. The platinum CE exhibits a J_{SC} of 14.47 mA cm^{-2}, a V_{OC} of 735 mV and a FF of 0.70, which result in a PCE of 7.44%. Between the platinum and SRO-GQD CEs, the SRO-GQD-based CE showed 8.05% PCE, which is much higher than those of platinum-based devices. The Nyquist plots of the dummy cells showed that the series resistance (R_s) of the SRO-GQD CE (3.84 Ω cm^2) is smaller than that of the $SrRuO_3$ CE (5.19 Ω cm^2). Moreover, SRO-GQD exhibits a lower charge-transfer impedance (R_{ct}; 9.30 Ω cm^2) than $SrRuO_3$ (12.09 Ω cm^2).

4.3 CD-based supercapacitors

Currently, in order to realise supercapacitors which exhibit higher electrochemical performances, many transition metal oxides (such as MnO_2, $Ni(OH)_2$ and Co_3O_4) are used for the electrode material. However, the relatively poor cycle-life of the transition metal oxide electrode restricts their application in electrochemical energy storage. Supercapacitors are reported to benefit from the use of CDs. According to the charge storage mechanism, supercapacitors can be classified into pseudo-capacitors (Faraday reactions) and double-layer capacitors (ion absorption).

The morphological and electronic properties of supercapacitors can be tuned through the surface areas, differently sized crystalline domains, and charge trapping centres. CDs may be a suitable precursor material for the fabrication of supercapacitors owing to their abundant "carbonisation" structures.[201] For example, Strauss and co-workers[201] synthesised porous graphene using CDs; the CDs were initially prepared by microwave-assisted thermolysis of CA and urea and subsequent annealing. Then, they transformed the CDs into 3D-turbostratic-graphene, which involved the reduction of CDs in a CDs/CO_2 plasma with the help of an infrared laser (Fig. 17a). The cyclic voltammogram of sthe 3D-turbostratic-graphene electrode revealed a pseudo-rectangular shape in the operating electrochemical window of 1, 5 and 10 V s^{-1}. The galvanostatic charge–discharge curves obtained at different current densities of 4, 10, 20, 40 and 100 A g^{-1} show good capacitive behaviour. Lv *et al.*[53] prepared a

3D multichannel aerogel of carbon QDs for supercapacitors. The CDs were synthesised by simple electrochemical preparation. Apart from acting as a precursor in the preparation of microporous structures, CDs can also induce other materials to form nano-rods and wires and other special structures. Xia's group[52] proposed the mechanism of CD-induced MnO_2 nanowire formation. The CDs were prepared *via* a one-step hydrothermal approach. Then, the CDs were added to $MnCl_2$ and $KMnO_4$ solutions and finally placed in a reactor at 160 °C for 10 h. They obtained a MnO_2 nanowire/CDs membrane. The flexible MnO_2 nanowire/CDs electrode exhibited a high specific capacitance of 340 F g^{-1} at 1 A g^{-1}, and, when the current density increased by 20 times (20 A g^{-1}), the loss in the specific capacitance was only 24% (260 F g^{-1}).

The presence of oxygen-containing functional groups in CDs makes them exhibit a strong hydrophilicity as an electrode material, which is advantageous for improving the wettability of the electrolyte and thereby enhancing the interfacial compatibility. However, the numerous oxygen-containing functional groups are harmful to the cycle life, electrochemical capacity, conductivity and stability of the electrode material, particularly at a high current density. Therefore, the original materials appropriately doped with CDs can form nanocomposites which can offer the advantage of high wettability and electrochemical properties of the electrolyte. Zhao *et al.*[202] designed an interconnected 3D network of reduced graphene oxide (rGO) nanosheets decorated with CDs. The rGO/CDs nanocomposites were fabricated by a one-pot hydrothermal method with GO and CDs (Fig. 17b). The experimental results show that the maximum specific capacitance of the rGO/CDs is 308 F g^{-1} when the current density is 0.5 A g^{-1}, which is much higher than that of the single CD system (2.2 F g^{-1}) and the single rGO system (200 F g^{-1}). Furthermore, excellent cycling stability was observed (92% of the capacitance remained after 20 000 charge/discharge cycles at a high current density of 10 A g^{-1}). In addition, Wei *et al.*[203] fabricated porous carbon materials for the negative electrode; the porous carbon material was derived from CDs and PAM hydrogels (Fig. 17c). This material was covered with electron-rich defects and functional groups, which are beneficial for the adsorption/reaction of cations. Contrast experiments showed that phosphorus, nitrogen, and oxygen co-doped materials display optimal surface elements, charge distributions, and pore size distributions in the structures. It indicated that heteroatom doping is conducive to the formation of electron-rich regions on the electrode surfaces. The obtained supercapacitors revealed energy densities of 62.8–90.1 W h kg^{-1} in different systems.

4.4 CD-based LIBs

The advantages of high working voltage, high capacity, long cycling life, and environmental benignity have provided LIBs with the opportunity to be widely used as secondary batteries, the market of which is developing beyond expectation.[57] Cathode, anode and electrolyte are the three important components affecting the performance of LIBs. The advantages of safety and inhibition of the formation of lithium dendrites of solid polymer electrolytes (SPEs)[204,205] can be beneficial to some special requirement in the preparation of new-generation energy storage devices. In addition to improving the safety, the electrochemical and thermal stability characteristics of SPEs allow LIBs to function at high temperatures and operating voltages. Ma *et al.*[206] fabricated PEO/CDs/$LiClO_4$ nanocomposite polymer electrolytes.

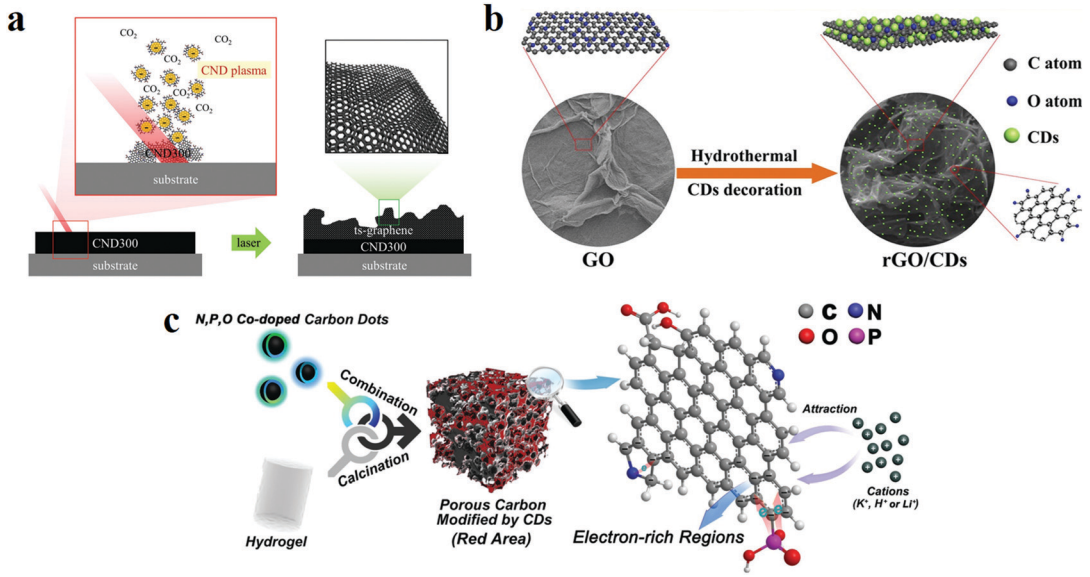

Fig. 17 (a) Schematic of the supercapacitor synthesised with porous graphene from CDs after irradiation with a high-power infrared laser beam; the CDs form a porous 3D-ts-graphene network. Reprinted with permission from ref. 201, Copyright 2018, Wiley-VCH Verlag GmbH & Co. KGaA. (b) Overall synthesis procedure of an interconnected 3D network of rGO decorated with CDs. Reprinted with permission from ref. 202, Copyright 2017, Wiley-VCH Verlag GmbH & Co. KGaA. (c) Schematic diagram of the preparation of a negative electrode by using CDs and a porous hydrogel. Reprinted with permission from ref. 203, Copyright 2019, Wiley-VCH Verlag GmbH & Co. KGaA.

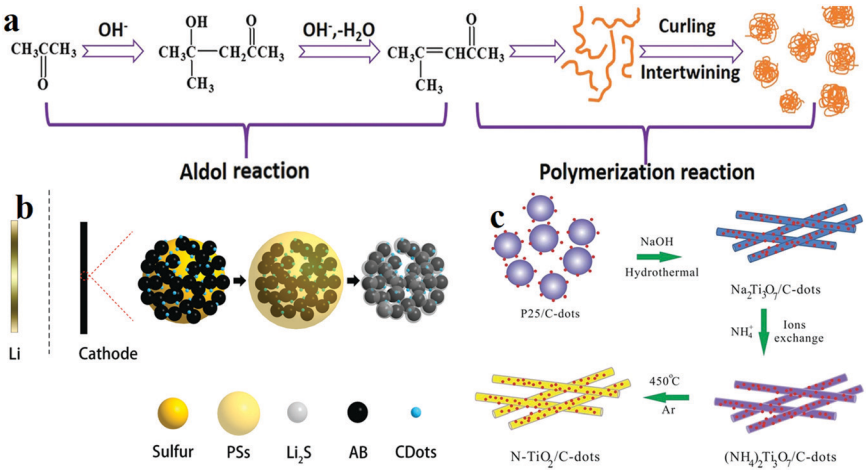

Fig. 18 Schematic diagram of the preparation of CD-based LIBs and their properties. (a–c): (a) synthesis of as-prepared CDs. Reprinted with permission from ref. 206, Copyright 2018, Wiley-VCH Verlag GmbH & Co. KGaA. (b) Illustrations of CD-based cathodes for lithium–sulfur batteries. Reprinted with permission from ref. 207, Copyright 2018, Wiley-VCH Verlag GmbH & Co. KGaA. (c) Illustration of the fabrication process to produce a N-TiO_2/CDs composite for the LIB anode. Reprinted with permission from ref. 208, Copyright 2015, The Royal Society of Chemistry.

The CDs were synthesised by the hydrothermal method (Fig. 18a). The PEO/CDs/$LiClO_4$ electrolyte showed a lithium transference number of 0.48 and an ionic conductivity of 1.39×10^{-4} S cm^{-1} at room temperature, which were higher than the corresponding values of PEO–Li (0.21). CDs promoted the dissociation of $LiClO_4$ salt, and the surface with oxygen-containing functional groups induced the adsorption of ClO_4^-, which reduced the crystallinity of the PEO matrix.

In the case of lithium–sulfur (Li–S) batteries, when the batteries are assembled under a high sulfur loading, as the thickness of the active layer increases, the resistance of the battery gradually increases, and the ion transport is blocked, which makes it difficult to achieve the theoretical level predicted by electrochemistry. In addition, the dissolution of polysulfide in the electrolyte easily occurs during charging and discharging, and polysulfide migrates to the anode side during the cycling. To overcome this problem, modification of the electrochemical interface by using CDs may be a good strategy of improving the battery system performance at the industrial scale. Hu and co-workers[207] fabricated PEI-functionalised CD (PEI-CDs)-modified cathodes. The CDs were synthesised by a one-pot carbonization method with PEI. The obtained PEI-CDs were then mixed with sulfur, acetylene black (AB), and polyvinylidene difluoride to form a PEI-CDs@AB/S cathode. During the discharging process, soluble polysulfides (LiPSs) result from the reduction of sulfur inside and/or around the cathode structure. At the end of the discharging process, the insoluble Li_2S was further reduced on the surface of PEI-CD-modified AB by soluble LiPSs. (Fig. 18b). The PEI-CDs@AB/S composite cathode exhibited an areal capacity of 3.3 mA h cm^{-2} under an areal sulfur loading of 6.6 mg cm^{-2}. Further, a high current density of 8 mA cm^{-2} was obtained, and the capacity decay rate was only 0.07% after 400 cycles or more; the retention capacity also significantly improved. By comparing the PEI-CDs@AB/S cathode with the AB/S cathode, it is found that the PEI-CD-doped cathode displays a better rate performance at a high current density. It delivers reversible areal capacities ranging from 4.7 mA h cm^{-2} at 2 mA cm^{-2} to 2.6 mA h cm^{-2} at 10 mA cm^{-2}, which are comparable to those of commercial LIBs (2–4 mA h cm^{-2}).

In addition, CDs are used as the anode material of LIBs. Yang *et al.*[208] fabricated a N-TiO_2 nanorods/CDs composite as an anode through hydrothermal and ion exchange processes and calcination (Fig. 18c). The cyclic behaviour of the N-TiO_2/CDs composite showed that the specific capacity is 262 and 202 mA h g^{-1} at 2C and 10C charging and discharging rates, respectively, and about 90% of the capacity is maintained after 1000 cycles. The initial reversible discharge specific capacities of pure N-TiO_2 at 2C and 10C are 203 and 147 mA h g^{-1}, respectively, and the retention rates after 1000 cycles are only 76.2% and 83.8%, respectively. Comparing the two composite materials, it can be found that the doping of CDs results in a better rate performance. When the composite material is charged at a high rate of 100C (36 s charging and discharging, 16.8 A g^{-1}), the specific capacity of pure N-TiO_2 rapidly drops to 36 mA h g^{-1} at the same rate, whereas a specific capacity of 116 mA h g^{-1} can be observed for N-TiO_2/CDs.

5. CDs for bioapplications

The application of CDs in biomedicine is one of the most frequently reported and discussed applications. With the exploration of CDs becoming more intensive, some challenges in the field of biomedical applications can be dealt with using CDs. High photostability, resistance to photobleaching, high sensitivity and low toxicity are characteristics of CDs which are highly significant in long-term bioimaging applications. In addition, an abundance of sources and selective modification render CDs easily applicable in nanomedicine.[46]

5.1 CD-based target-specific bioimaging

Since scientists discovered fluorescent proteins such as green fluorescent proteins,[209] biological fluorescent materials have

become important imaging tools for studying objects/systems. However, poor photostability and the difficulty in labelling cells or other microorganisms of bioluminescent proteins limit their application as long-term imaging tools. sQDs have long been considered to be promising for bioimaging owing to their excellent PL properties. However, the high toxicity and poor solubility of traditional QDs have limited their bioimaging application in living cells and organisms. In this context, the excellent PL properties and biocompatibility have rendered CDs the perfect material for new-generation bioimaging, especially for target-specific imaging, in recent years. In the study by He and co-workers, arginyl-glycyl-aspartic acid (RGD) peptides were attached to CDs (RGD-CDs) to target integrin receptors on live cell membranes. It is seen that the fluorescence signal of the HeLa cells labelled with RGD-CDs can be detected under excitation with 405 and 488 nm lasers. In contrast, the fluorescence signal does not appear for a human breast adenocarcinoma (MCF-7) cell incubated with the same concentration of RGD-CDs, which indicates specific targeting of live cells by RGD-CDs. Because of the hindrance presented by the cell membrane, CDs find it difficult to reach the nuclei and image them. In order to overcome this difficulty, Yang *et al.*[210] fabricated CDs by using a nuclear localisation signal (NLS) peptide, which is capable of targeted imaging of the cell nucleus. *In vitro* cytotoxicity experiments led to the conclusion that CDs and NLS-modified CDs (NLS-CDs) are biocompatible. In addition, intracellular localisation experiments on MCF-7 and adenocarcinomic human alveolar basal epithelial (A549) cells demonstrated that NLS-CDs can penetrate the cell tissue to enter the nucleus and emit blue light, which showed that CDs can be used as a target probe in nuclear imaging. In addition, the other components of the cell can also be marked by selecting the specific target and suitably modifying CDs. For example, Zhang *et al.*[211] reported mitochondria-targeting CDs. They used magnetic mesoporous silica nanoparticles (Fe_3O_4@mSiO_2) to modify the surface of triphenylphosphine (TPP) and then combined it with fluorescent CDs to prepare biocompatible target fluorescent probes. The as-prepared nanoprobe revealed

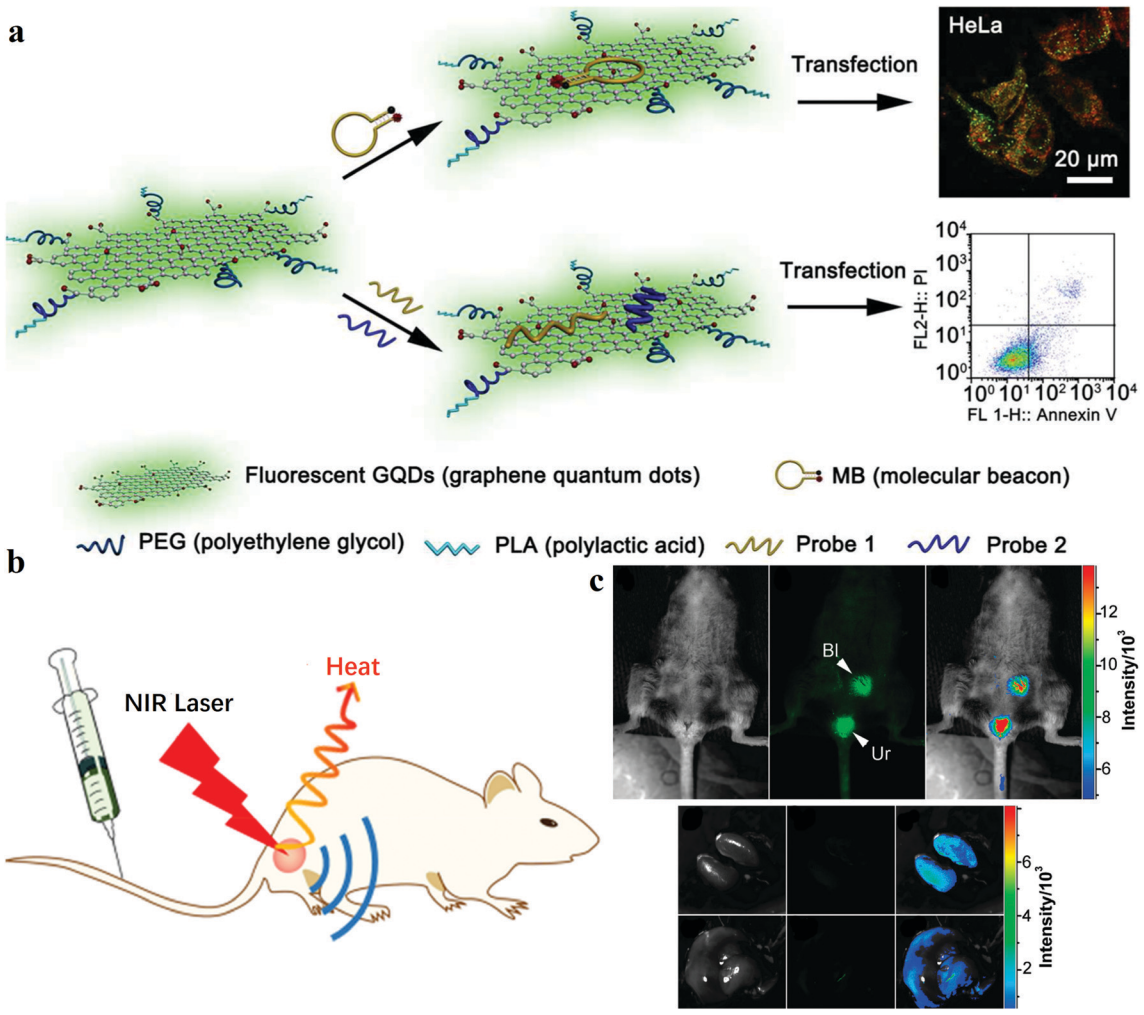

Fig. 19 Application of CDs in bioimaging. (a) Schematic illustration of the preparation of GQDs for cell imaging and combined delivery of specific gene-targeting agents. Reprinted with permission from ref. 214, Copyright 2015, American Chemical Society. (b) Schematic illustrating the fabrication of CuCD NSs and their application in multimodal imaging. Reprinted with permission from ref. 217, Copyright 2018, American Chemical Society. (c) Intravenous injection of mice imaged with CDs. Reprinted with permission from ref. 16, Copyright 2009, American Chemical Society.

low mitochondria-targeting cytotoxicity in various cell lines such as CHO, A549, SH-SY5Y, HeLa, HFF and HMEC-1. In addition, Wu *et al.*[212] also used TPP to modify CDs to selectively label mitochondria and probe the peroxynitrite in living cells. Wang and co-workers[213] prepared ultra-stable sulfonated GQDs for Golgi apparatus imaging. They chose HeLa cells and MCF-7 cells as the model for their biological experiments. The GQDs display high target-specificity towards the Golgi apparatus in HeLa and MCF7 cancer cells when observed under a traditional fluorescence microscope. MicroRNAs (miRNAs), as a class of endogenous non-coding RNAs, participate in many regulatory pathways in eukaryotes. For example, Dong *et al.*[214] fabricated GQD modified with PEG and poly(L-lactide) (PLA) for intracellular miRNA imaging. PEG and PLA render GQDs extremely biostable and optically stable, which is essential for intracellular imaging (Fig. 19a). Apart from their application in *in vitro* cellular imaging, CDs also display huge potential in *in vivo* imaging. In 2009, Yang *et al.*[16] first studied CDs for *in vivo* optical imaging. They synthesised CDs and C_{ZnS} dots. Comparison of the two types of CDs through *in vivo* imaging of mice included the axillary lymph node, kidneys and liver (Fig. 19c). With the addition of ZnS,[215] the *in vivo* imaging effect of mice of CDs was significantly improved. Because NIR light has the ability to penetrate tissues deeper and decrease the auto fluorescent background, it is ideal for *in vivo* imaging. For instance, Tao *et al.*[216] reported *in vivo* NIR fluorescence imaging by using CDs. They subcutaneously administered CDs to a nude mouse at three different locations, and NIR fluorescence was observed. Because CDs can be used for imaging multiple in vivo organs, it is possible to prepare targeted CDs for the detection of cancer cells. In addition, Wu and co-workers fabricated copper/CD-crosslinked nanosheets (CuCD NSs) by the hydrothermal method with copper ions and sulfur-doped CDs. The modified CuCD NSs exhibited lysosomal escape, nuclear targeting and laser-triggered cytosolic delivery, which could be used in multimodal imaging-guided cancer therapy (Fig. 19b).[217] Liu and co-workers[218] reported folate-CDs (FA-CDs) nanocomposites as a turn-on fluorescence probe for detecting cancer cells. Folate receptor (FR)-positive cancer cells could be distinguished with the FA-CDs probe in different cells. However, the FA-CDs probe is not used in *in vivo* imaging based on bioimaging experiments. Subsequently, Zheng *et al.*[219] fabricated CDs targeted toward brain cancer glioma by a pyrolysis approach. These CDs could reach the target and treat C6 glioma cells without the addition of any target molecules. In mice bioimaging experiments, the intensity of the fluorescence signal from the glioma site is much higher than that from a normal brain, which indicates that CDs can easily penetrate the blood–brain barrier and reach the glioma tissue.

5.2 CD-based nanomedicine

Drug delivery refers to safe and effective treatment which involves carrying the medicine to a particular location in the body and releasing it in a sustained manner. Many innovative materials such as polymers,[220] polymeric micelles,[221] liposomes,[222] QDs and carbon-based nanomaterials have found wide applications in drug delivery. Among them, the good biocompatibility and the surface drug loading capacity of CDs render it fit for application in the drug delivery field. Promising studies using CDs as nanocarriers for the delivery of various agents such as gene[223,224] and neurodisease drugs[225] have been reported. Zeng *et al.*[226] synthesised CDs rich in carboxyl groups and conjugated them with the anti-cancer drug doxorubicin (DOX) *via* a non-covalent bonding effect. Owing to the differences in pH between tumour cells and normal cells, DOX release can be regulated based on pH to target cancer cells.

In addition, Tang *et al.*[227] reported multifunctional FRET-based CDs for real-time monitoring of drug delivery and two-photon imaging. The obtained FRET-CDs drug delivery system has shown an excellent drug release efficiency and delivery targeted at tumour cells. Moreover, the fluorescence peak shift caused by FRET can be used to effectively monitor the sustained release of DOX in real time (Fig. 20a). Feng *et al.*[228] demonstrated charge-convertible CDs for imaging-guided drug delivery. The properties corresponding to the imaging-guided drug delivery of cisplatin(IV) prodrug-loaded charge-convertible CDs (CDs-Pt(IV)@PEG-(PAH/DMMA)) were studied. In a weakly acidic tumour cell microenvironment (pH ~ 6.8), the anionic polymer of PEG-(PAH/DMMA) can be converted to a cationic polymer, which leads to the release of positive CDs-Pt(IV). Moreover, because of the negative charge on the surface of the cancer cell membrane, the positively charged nanocarrier displays a high affinity towards it, so that the carrier and the

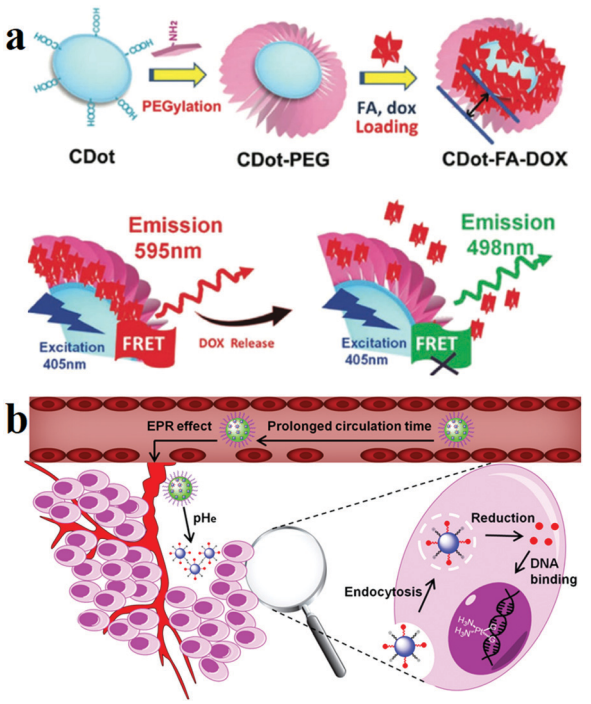

Fig. 20 (a) Schematic diagram of FRET monitoring drug delivery. Reprinted with permission from ref. 227, Copyright 2013, Wiley-VCH Verlag GmbH & Co. KGaA. (b) Schematic illustration of the targeting and treatment of cancer cells by using charge-changed CDs. Reprinted with permission from ref. 228, Copyright 2016, American Chemical Society.

cancer cells are more tightly bound, which is beneficial for sustained release of the drug. *In vitro* experiments confirmed that these charge-transformed CDs exhibit a higher target selectivity and a stronger therapeutic effect on tumour cells (Fig. 20b). Photodynamic therapy (PDT) is a highly effective, non-invasive method of cancer therapy, the principle of which is to convert O_2 into cytotoxic reactive oxygen species. Zheng *et al.*[229] prepared CD-decorated C_3N_4 nanoparticles to enhance PDT to fight against hypoxic tumours. C_3N_4 was chosen as a promising water splitting material. In addition, they assembled PpIX-PEG-RGD (an amphipathic polymer consisting of the photosensitiser protoporphyrin IX (PpIX) and the tumour-targeting sequence RGD, with PEG acting as the linker) and C_3N_4 to obtain polymer-modified CD carbon nitride nanoparticles (PCCN). A 630 nm laser can be used to induce the tumour-targeting PCCN to split water to generate O_2, which reaches and accumulates in the tumour tissue. In addition, the produced O_2 is converted into cytotoxic singlet oxygen ($^1O_2$) by the action of the photosensitiser, thereby achieving the purpose of treating cancer.

6. Conclusion and perspectives

Compared with the toxic metal QDs, CDs are promising material owing to their biocompatibility and great optical properties, which render them indispensable, especially in the optical, energy and biology fields. Recently, CDs have triggered numerous investigations with regard to their synthetic strategy, mechanism and basic properties. In this review, the effects of synthesis process, precursors, passivation and doping with heteroatoms on the properties of CDs were revealed. Among the synthesis strategies of CDs, hydrothermal is the most popular method, owing to its convenient, environment-friendly and inexpensive nature. Moreover, passivation and heteroatom doping can improve the QY, dispersibility and other properties of CDs. Some basic properties of CDs were discussed, including the optical, dispersibility and biocompatibility properties. Additionally, there are several applications of CDs which can potentially be developed. Anti-counterfeiting and data security are a novel application of CDs. Multiple models of security encryption technology have been developed, such as those based on fluorescence, phosphorescence and solvent and thermal treatment. The next step in CD security encryption is to explore a combined multi-technology for the protection of confidential papers and design of anti-counterfeit labels. Moreover, in combination with new detection equipment, a higher-level conceptual innovation security encryption design may be the trend of the future.

In addition, other optical and optoelectronic applications were reported for CD-based materials, such as sensing and LEDs. CDs revealed excellent properties in sensing and luminescence. On the other hand, the highlight of CDs being chiral was also reported. Furthermore, the applications of chiral CDs in biology and catalysis based on controlling the enzyme activity and cellular energy metabolism were also presented.[175,177,179] However, the narrow-band chiral signal and the difficulty in realising circularly polarised emission have limited their optoelectronic applications.[18] Therefore, the focus of future research should be in obtaining visible and even NIR range CD chiral signals and circularly polarised emission. Resolution of these issues may lead to a revolution in flat-panel displays.[230] The roles of CDs in energy applications such as photocatalysts, solar photovoltaics, supercapacitors and LIBs are emerging. While still in their infancy, CDs have shown much promise as individual or co-dependent components within various PV architectures, supercapacitors and batteries, with their roles ranging from sensitisers, charge carrier layers/films or tunnel junctions in solar cells to electrodes or electrolytes in supercapacitors and batteries.[196,197,206,231] Solving the issues of inferior broadband absorption and charge conductivity of CDs is the key to increasing their energy applications. Although their excellent properties conform to the scientific requirements, their high cost and low yield hinder their large-scale production. Hence, improving the synthesis strategy and preparing CDs with good repeatability and excellent performance has become the main research goal. Even so, CDs still exhibit significant (and perhaps yet-undiscovered) potential as inexpensive and sustainable alternatives in the pursuit of low-cost, high-performance energy harvesting and storage systems. Owing to the excellent PL and multi-coloured fluorescence characteristics, along with their non-toxic nature, CDs have increasingly been used in *in vitro* and *in vivo* bioimaging. Additionally, the composite system prepared by loading drugs with CDs provides a new idea for targeted identification and treatment of cancer cells. Although there are many bio-applications in which CDs have been shown to work, researchers should provide more pieces of evidence to prove that CD-based drugs are superior to traditional drugs in terms of their metabolic capacity. Therefore, the future research direction of CD-based drugs is to reduce the non-specific uptake of CDs by normal cells, and, at the same time, increase the specific ability to target cancer cells, increase the therapeutic effect and improve blood circulation. This CD-based targeted cancer treatment technology can effectively reduce the side effects, enhance specific treatment and trigger a revolution in disease prevention, diagnosis and treatment.[216,228]

After more than a decade of research on CDs, scientists have a deeper understanding of their fundamental properties. However, there still exist many challenges and debatable issues which must be addressed, such as band gap tuning and emission wavelength control. Before the wide application of CDs in diverse fields, the following critical issues must be addressed as part of future research: (1) better understanding of the PL mechanisms. Unlike QDs, the origin of fluorescence in CDs is unclear and questionable. Numerous studies have revealed different mechanisms in this regard, which can be attributed to the use of different conditions and starting materials. For example, Zhang *et al.*[232] prepared CDs by using molecules with fluorescent properties as precursors, and compared the fluorescence properties of the obtained CDs and precursors. The results showed that the obtained CDs display similar optical properties as the precursors of known chemical structure and characteristics.

(2) Establishment of a systematic synthesis protocol. Although a variety of CDs have been reported, and most of the obtained CDs exhibit PL properties, the spectral region of the fluorescence groups on their surface is wide, which means that the optical properties of the fluorescence groups cannot be accurately determined structurally. It may be because of the use of non-controllable precursors and non-standard synthetic pathways. For large-scale production of CDs, in order to precisely regulate the PL performance, the effects of different synthetic factors on the performance of CDs should be first determined by experiments, and then, the standard synthetic purification scheme for CDs should be established. (3) QY improvement and expansion of the spectral coverage. Although there are ways to increase the QY of CDs, a majority of CDs showed lower QYs, compared with those of QDs. With this in mind, it is necessary to first study the factors affecting the QY of CDs and subsequently develop strategies to improve it. At the same time, the research should also focus on extending the spectral range of CDs to longer wavelengths. In summary, as a new member of the carbon material universe, CDs find potential applications in many fields owing to their excellent optical and physical properties and quantum size effects. It is believed that with further research, more applications of CDs can be developed in the future. CDs have also revealed their novel performance and potential in practical applications in recent years. It is believed that CDs can replace the traditional materials in various fields, which can lead to the development of more applications in the future.

Conflicts of interest

The authors have no conflicts of interest to declare.

Acknowledgements

This work was financially supported by the National Key R&D Program of China (No. 2016YFA0202302), the National Natural Science Funds for Distinguished Young Scholars (No. 51425306), the State Key Program of National Natural Science Foundation of China (No. 51633007), and the National Natural Science Foundation of China (No. 51573125, 51573147 and 51803151).

References

1 B.-T. Zhang, X. Zheng, H.-F. Li and J.-M. Lin, *Anal. Chim. Acta*, 2013, **784**, 1–17.
2 J. McClure, *Phys. Rev.*, 1956, **104**, 666.
3 E. Taft and H. Philipp, *Phys. Rev.*, 1965, **138**, A197.
4 B. C. Thompson and J. M. Fréchet, *Angew. Chem., Int. Ed.*, 2008, **47**, 58–77.
5 J. Liu, A. G. Rinzler, H. Dai, J. H. Hafner, R. K. Bradley, P. J. Boul, A. Lu, T. Iverson, K. Shelimov and C. B. Huffman, *Science*, 1998, **280**, 1253–1256.
6 M. S. Dresselhaus, G. Dresselhaus, P. Eklund and A. Rao, *The physics of fullerene-based and fullerene-related materials*, Springer, Dordrecht, 2000, pp. 331–379.
7 S. J. Tans, A. R. Verschueren and C. Dekker, *Nature*, 1998, **393**, 49.
8 W. A. De Heer, A. Chatelain and D. Ugarte, *Science*, 1995, **270**, 1179–1180.
9 E. T. Thostenson, Z. Ren and T.-W. Chou, *Compos. Sci. Technol.*, 2001, **61**, 1899–1912.
10 Y. Hernandez, V. Nicolosi, M. Lotya, F. M. Blighe, Z. Sun, S. De, I. McGovern, B. Holland, M. Byrne and Y. K. Gun'Ko, *Nat. Nanotechnol.*, 2008, **3**, 563.
11 S. Stankovich, D. A. Dikin, G. H. Dommett, K. M. Kohlhaas, E. J. Zimney, E. A. Stach, R. D. Piner, S. T. Nguyen and R. S. Ruoff, *Nature*, 2006, **442**, 282.
12 W. Feng, P. Long, Y. Feng and Y. Li, *Adv. Sci.*, 2016, **3**, 1500413.
13 X. Xu, R. Ray, Y. Gu, H. J. Ploehn, L. Gearheart, K. Raker and W. A. Scrivens, *J. Am. Chem. Soc.*, 2004, **126**, 12736–12737.
14 Y.-P. Sun, B. Zhou, Y. Lin, W. Wang, K. S. Fernando, P. Pathak, M. J. Meziani, B. A. Harruff, X. Wang and H. Wang, *J. Am. Chem. Soc.*, 2006, **128**, 7756–7757.
15 H. Liu, T. Ye and C. Mao, *Angew. Chem., Int. Ed.*, 2007, **46**, 6473–6475.
16 S.-T. Yang, L. Cao, P. G. Luo, F. Lu, X. Wang, H. Wang, M. J. Meziani, Y. Liu, G. Qi and Y.-P. Sun, *J. Am. Chem. Soc.*, 2009, **131**, 11308–11309.
17 S. Zhu, Q. Meng, L. Wang, J. Zhang, Y. Song, H. Jin, K. Zhang, H. Sun, H. Wang and B. Yang, *Angew. Chem., Int. Ed.*, 2013, **52**, 3953–3957.
18 L. Ethordevic, F. Arcudi, A. D'Urso, M. Cacioppo, N. Micali, T. Burgi, R. Purrello and M. Prato, *Nat. Commun.*, 2018, **9**, 3442.
19 F. Yuan, T. Yuan, L. Sui, Z. Wang, Z. Xi, Y. Li, X. Li, L. Fan, Z. Tan, A. Chen, M. Jin and S. Yang, *Nat. Commun.*, 2018, **9**, 2249.
20 A. P. Alivisatos, *Science*, 1996, **271**, 933–937.
21 D. Loss and D. P. DiVincenzo, *Phys. Rev. A: At., Mol., Opt. Phys.*, 1998, **57**, 120.
22 A. M. Derfus, W. C. Chan and S. N. Bhatia, *Nano Lett.*, 2004, **4**, 11–18.
23 X. Li, M. Rui, J. Song, Z. Shen and H. Zeng, *Adv. Funct. Mater.*, 2015, **25**, 4929–4947.
24 M. Kaur, M. Kaur and V. K. Sharma, *Adv. Colloid Interface Sci.*, 2018, **259**, 44–64.
25 J. B. Essner and G. A. Baker, *Environ. Sci.: Nano*, 2017, **4**, 1216–1263.
26 F. Yuan, Z. Wang, X. Li, Y. Li, Z. Tan, L. Fan and S. Yang, *Adv. Mater.*, 2017, **29**, 1604436.
27 S. Sahu, B. Behera, T. K. Maiti and S. Mohapatra, *Chem. Commun.*, 2012, **48**, 8835–8837.
28 B. Zhu, S. Sun, Y. Wang, S. Deng, G. Qian, M. Wang and A. Hu, *J. Mater. Chem. C*, 2013, **1**, 580–586.
29 K. Jiang, S. Sun, L. Zhang, Y. Lu, A. Wu, C. Cai and H. Lin, *Angew. Chem., Int. Ed.*, 2015, **54**, 5360–5363.
30 C. Wang, B. Xu, M. Li, Z. Chi, Y. Xie, Q. Li and Z. Li, *Mater. Horiz.*, 2016, **3**, 220–225.

31 M. Fu, F. Ehrat, Y. Wang, K. Z. Milowska, C. Reckmeier, A. L. Rogach, J. K. Stolarczyk, A. S. Urban and J. Feldmann, *Nano Lett.*, 2015, **15**, 6030–6035.
32 N. Dhenadhayalan, K.-C. Lin, R. Suresh and P. Ramamurthy, *J. Phys. Chem. C*, 2016, **120**, 1252–1261.
33 A. Cayuela, M. Soriano, C. Carrillo-Carrion and M. Valcarcel, *Chem. Commun.*, 2016, **52**, 1311–1326.
34 M. J. Krysmann, A. Kelarakis, P. Dallas and E. P. Giannelis, *J. Am. Chem. Soc.*, 2011, **134**, 747–750.
35 L. Wang, K. G. Gutierrez-Cuevas, A. Urbas and Q. Li, *Adv. Opt. Mater.*, 2016, **4**, 247–251.
36 H. Sun, S. Liu, W. Lin, K. Y. Zhang, W. Lv, X. Huang, F. Huo, H. Yang, G. Jenkins and Q. Zhao, *Nat. Commun.*, 2014, **5**, 3601.
37 X. Hou, C. Ke, C. J. Bruns, P. R. McGonigal, R. B. Pettman and J. F. Stoddart, *Nat. Commun.*, 2015, **6**, 6884.
38 A. P. Kulkarni, C. J. Tonzola, A. Babel and S. A. Jenekhe, *Chem. Mater.*, 2004, **16**, 4556–4573.
39 Y. Ling, Z. Yuan, Y. Tian, X. Wang, J. C. Wang, Y. Xin, K. Hanson, B. Ma and H. Gao, *Adv. Mater.*, 2016, **28**, 305–311.
40 X. Sun and Y. Lei, *TrAC, Trends Anal. Chem.*, 2017, **89**, 163–180.
41 J. Zhang and S.-H. Yu, *Mater. Today*, 2016, **19**, 382–393.
42 R. Wang, K.-Q. Lu, Z.-R. Tang and Y.-J. Xu, *J. Mater. Chem. A*, 2017, **5**, 3717–3734.
43 F. Zhai, Y. Feng, K. Zhou, L. Wang, Z. Zheng and W. Feng, *J. Mater. Chem. C*, 2019, **7**, 2146–2171.
44 Z.-g. Zheng, Y. Li, H. K. Bisoyi, L. Wang, T. J. Bunning and Q. Li, *Nature*, 2016, **531**, 352.
45 M. L. Liu, B. B. Chen, C. M. Li and C. Z. Huang, *Green Chem.*, 2019, **21**, 449–471.
46 Z. Peng, X. Han, S. Li, A. O. Al-Youbi, A. S. Bashammakh, M. S. El-Shahawi and R. M. Leblanc, *Coord. Chem. Rev.*, 2017, **343**, 256–277.
47 J. Zhou, H. Zhou, J. Tang, S. Deng, F. Yan, W. Li and M. Qu, *Microchim. Acta*, 2017, **184**, 343–368.
48 Q. Liu, B. Guo, Z. Rao, B. Zhang and J. R. Gong, *Nano Lett.*, 2013, **13**, 2436–2441.
49 A. Tan, L. Yildirimer, J. Rajadas, H. D. L. Peña, G. Pastorin and A. Seifalian, *Nanomedicine*, 2011, **6**, 1101–1114.
50 P. Namdari, B. Negahdari and A. Eatemadi, *Biomed. Pharmacother.*, 2017, **87**, 209–222.
51 G. A. M. Hutton, B. C. M. Martindale and E. Reisner, *Chem. Soc. Rev.*, 2017, **46**, 6111–6123.
52 H. Lv, X. Gao, Q. Xu, H. Liu, Y. G. Wang and Y. Xia, *ACS Appl. Mater. Interfaces*, 2017, **9**, 40394–40403.
53 L. Lv, Y. Fan, Q. Chen, Y. Zhao, Y. Hu, Z. Zhang, N. Chen and L. Qu, *Nanotechnology*, 2014, **25**, 235401.
54 R. Genc, M. O. Alas, E. Harputlu, S. Repp, N. Kremer, M. Castellano, S. G. Colak, K. Ocakoglu and E. Erdem, *Sci. Rep.*, 2017, **7**, 11222.
55 J. Lin, Y. Yuan, Q. Su, A. Pan, S. Dinesh, C. Peng, G. Cao and S. Liang, *Electrochim. Acta*, 2018, **292**, 63–71.
56 M. Jing, J. Wang, H. Hou, Y. Yang, Y. Zhang, C. Pan, J. Chen, Y. Zhu and X. Ji, *J. Mater. Chem. A*, 2015, **3**, 16824–16830.
57 M. S. Balogun, Y. Luo, F. Lyu, F. Wang, H. Yang, H. Li, C. Liang, M. Huang, Y. Huang and Y. Tong, *ACS Appl. Mater. Interfaces*, 2016, **8**, 9733–9744.
58 J. Lu, J.-x. Yang, J. Wang, A. Lim, S. Wang and K. P. Loh, *ACS Nano*, 2009, **3**, 2367–2375.
59 L. Zheng, Y. Chi, Y. Dong, J. Lin and B. Wang, *J. Am. Chem. Soc.*, 2009, **131**, 4564–4565.
60 A. C. Dillon, K. Jones, T. Bekkedahl, C. Kiang, D. Bethune and M. Heben, *Nature*, 1997, **386**, 377.
61 M. J. O'connell, S. M. Bachilo, C. B. Huffman, V. C. Moore, M. S. Strano, E. H. Haroz, K. L. Rialon, P. J. Boul, W. H. Noon and C. Kittrell, *Science*, 2002, **297**, 593–596.
62 V. Nguyen, L. Yan, J. Si and X. Hou, *J. Appl. Phys.*, 2015, **117**, 084304.
63 S. Hu, J. Liu, J. Yang, Y. Wang and S. Cao, *J. Nanopart. Res.*, 2011, **13**, 7247–7252.
64 S. Kulinich, T. Kondo, Y. Shimizu and T. Ito, *J. Appl. Phys.*, 2013, **113**, 033509.
65 T. Tsuji, D.-H. Thang, Y. Okazaki, M. Nakanishi, Y. Tsuboi and M. Tsuji, *Appl. Surf. Sci.*, 2008, **254**, 5224–5230.
66 T. E. Itina, *J. Phys. Chem. C*, 2010, **115**, 5044–5048.
67 J. Zhou, C. Booker, R. Li, X. Zhou, T.-K. Sham, X. Sun and Z. Ding, *J. Am. Chem. Soc.*, 2007, **129**, 744–745.
68 D. B. Shinde and V. K. Pillai, *Chem. – Eur. J.*, 2012, **18**, 12522–12528.
69 H. Ming, Z. Ma, Y. Liu, K. Pan, H. Yu, F. Wang and Z. Kang, *Dalton Trans.*, 2012, **41**, 9526–9531.
70 A. Ananthanarayanan, X. Wang, P. Routh, B. Sana, S. Lim, D.-H. Kim, K.-H. Lim, J. Li and P. Chen, *Adv. Funct. Mater.*, 2014, **24**, 3021–3026.
71 R. Ye, C. Xiang, J. Lin, Z. Peng, K. Huang, Z. Yan, N. P. Cook, E. L. Samuel, C. C. Hwang, G. Ruan, G. Ceriotti, A. R. Raji, A. A. Marti and J. M. Tour, *Nat. Commun.*, 2013, **4**, 2943.
72 L. Cao, X. Wang, M. J. Meziani, F. Lu, H. Wang, P. G. Luo, Y. Lin, B. A. Harruff, L. M. Veca and D. Murray, *J. Am. Chem. Soc.*, 2007, **129**, 11318–11319.
73 S. Zhu, X. Zhao, Y. Song, S. Lu and B. Yang, *Nano Today*, 2016, **11**, 128–132.
74 H. He, X. Wang, Z. Feng, T. Cheng, X. Sun, Y. Sun, Y. Xia, S. Wang, J. Wang and X. Zhang, *J. Mater. Chem. B*, 2015, **3**, 4786–4789.
75 X. Wang, K. Qu, B. Xu, J. Ren and X. Qu, *J. Mater. Chem.*, 2011, **21**, 2445–2450.
76 X. Zhai, P. Zhang, C. Liu, T. Bai, W. Li, L. Dai and W. Liu, *Chem. Commun.*, 2012, **48**, 7955–7957.
77 Z. Ma, H. Ming, H. Huang, Y. Liu and Z. Kang, *New J. Chem.*, 2012, **36**, 861–864.
78 S. Zhuo, M. Shao and S.-T. Lee, *ACS Nano*, 2012, **6**, 1059–1064.
79 W. Kwon, S. Do and S.-W. Rhee, *RSC Adv.*, 2012, **2**, 11223.
80 Y. Yang, D. Wu, S. Han, P. Hu and R. Liu, *Chem. Commun.*, 2013, **49**, 4920–4922.
81 Y. Liu, Q. Zhou, J. Li, M. Lei and X. Yan, *Sens. Actuators, B*, 2016, **237**, 597–604.
82 S. Lu, X. Zhao, S. Zhu, Y. Song and B. Yang, *Nanoscale*, 2014, **6**, 13939–13944.

83 R. Atchudan, T. N. J. I. Edison and Y. R. Lee, *J. Colloid Interface Sci.*, 2016, **482**, 8–18.
84 V. N. Mehta, S. Jha, H. Basu, R. K. Singhal and S. K. Kailasa, *Sens. Actuators, B*, 2015, **213**, 434–443.
85 Y. Guo, L. Zhang, F. Cao and Y. Leng, *Sci. Rep.*, 2016, **6**, 35795.
86 J. Xu, T. Lai, Z. Feng, X. Weng and C. Huang, *Luminescence*, 2015, **30**, 420–424.
87 V. Ramanan, B. Siddaiah, K. Raji and P. Ramamurthy, *ACS Sustainable Chem. Eng.*, 2018, **6**, 1627–1638.
88 Y. Hu, J. Yang, J. Tian, L. Jia and J.-S. Yu, *Carbon*, 2014, **77**, 775–782.
89 S. Y. Park, H. U. Lee, E. S. Park, S. C. Lee, J.-W. Lee, S. W. Jeong, C. H. Kim, Y.-C. Lee, Y. S. Huh and J. Lee, *ACS Appl. Mater. Interfaces*, 2014, **6**, 3365–3370.
90 F. Niu, Y. Xu, M. Liu, J. Sun, P. Guo and J. Liu, *Nanoscale*, 2016, **8**, 5470–5477.
91 Y.-Q. Zhang, D.-K. Ma, Y. Zhuang, X. Zhang, W. Chen, L.-L. Hong, Q.-X. Yan, K. Yu and S.-M. Huang, *J. Mater. Chem.*, 2012, **22**, 16714.
92 Y. Dong, H. Pang, H. B. Yang, C. Guo, J. Shao, Y. Chi, C. M. Li and T. Yu, *Angew. Chem., Int. Ed.*, 2013, **52**, 7800–7804.
93 H. Fei, R. Ye, G. Ye, Y. Gong, Z. Peng, X. Fan, E. L. Samuel, P. M. Ajayan and J. M. Tour, *ACS Nano*, 2014, **8**, 10837–10843.
94 Y. P. Sun, X. Wang, F. Lu, L. Cao, M. J. Meziani, P. G. Luo, L. Gu and L. M. Veca, *J. Phys. Chem. C*, 2008, **112**, 18295–18298.
95 L. Tang, R. Ji, X. Cao, J. Lin, H. Jiang, X. Li, K. S. Teng, C. M. Luk, S. Zeng, J. Hao and S. P. Lau, *ACS Nano*, 2012, **6**, 5102–5110.
96 D. Li, P. Jing, L. Sun, Y. An, X. Shan, X. Lu, D. Zhou, D. Han, D. Shen and Y. Zhai, *Adv. Mater.*, 2018, **30**, 1705913.
97 S. Qu, D. Zhou, D. Li, W. Ji, P. Jing, D. Han, L. Liu, H. Zeng and D. Shen, *Adv. Mater.*, 2016, **28**, 3516–3521.
98 W. Wang, B. Wang, H. Embrechts, C. Damm, A. Cadranel, V. Strauss, M. Distaso, V. Hinterberger, D. M. Guldi and W. Peukert, *RSC Adv.*, 2017, **7**, 24771–24780.
99 Y. Xiong, J. Schneider, C. J. Reckmeier, H. Huang, P. Kasak and A. L. Rogach, *Nanoscale*, 2017, **9**, 11730–11738.
100 S. Zhu, Y. Song, X. Zhao, J. Shao, J. Zhang and B. Yang, *Nano Res.*, 2015, **8**, 355–381.
101 Y. Xu, M. Wu, Y. Liu, X. Z. Feng, X. B. Yin, X. W. He and Y. K. Zhang, *Chem. – Eur. J.*, 2013, **19**, 2276–2283.
102 J. Shen, Y. Zhu, C. Chen, X. Yang and C. Li, *Chem. Commun.*, 2011, **47**, 2580–2582.
103 L. Wang, H. Dong, Y. Li, C. Xue, L.-D. Sun, C.-H. Yan and Q. Li, *J. Am. Chem. Soc.*, 2014, **136**, 4480–4483.
104 D. Tan, S. Zhou and J. Qiu, *ACS Nano*, 2012, **6**, 6530–6531.
105 M. Shao and S. Zhuo, *ACS Nano*, 2012, **6**, 6532.
106 Z. Gan, X. Wu, G. Zhou, J. Shen and P. K. Chu, *Adv. Opt. Mater.*, 2013, **1**, 554–558.
107 K. Jiang, L. Zhang, J. Lu, C. Xu, C. Cai and H. Lin, *Angew. Chem., Int. Ed.*, 2016, **55**, 7231–7235.
108 F. Wang, S. Pang, L. Wang, Q. Li, M. Kreiter and C.-Y. Liu, *Chem. Mater.*, 2010, **22**, 4528–4530.
109 M. Han, S. Zhu, S. Lu, Y. Song, T. Feng, S. Tao, J. Liu and B. Yang, *Nano Today*, 2018, **19**, 201–218.
110 P. Long, Y. Feng, Y. Li, C. Cao, S. Li, H. An, C. Qin, J. Han and W. Feng, *ACS Appl. Mater. Interfaces*, 2017, **9**, 37981–37990.
111 W. Wei, C. Xu, L. Wu, J. Wang, J. Ren and X. Qu, *Sci. Rep.*, 2014, **4**, 3564.
112 H. Tetsuka, R. Asahi, A. Nagoya, K. Okamoto, I. Tajima, R. Ohta and A. Okamoto, *Adv. Mater.*, 2012, **24**, 5333–5338.
113 Y. Dong, C. Chen, X. Zheng, L. Gao, Z. Cui, H. Yang, C. Guo, Y. Chi and C. M. Li, *J. Mater. Chem.*, 2012, **22**, 8764–8766.
114 H. Ding, S. B. Yu, J. S. Wei and H. M. Xiong, *ACS Nano*, 2016, **10**, 484–491.
115 S. Hu, A. Trinchi, P. Atkin and I. Cole, *Angew. Chem., Int. Ed.*, 2015, **54**, 2970–2974.
116 L. Bao, C. Liu, Z. L. Zhang and D. W. Pang, *Adv. Mater.*, 2015, **27**, 1663–1667.
117 L. Han, S. G. Liu, J. X. Dong, J. Y. Liang, L. J. Li, N. B. Li and H. Q. Luo, *J. Mater. Chem. C*, 2017, **5**, 10785–10793.
118 J. Zhu, X. Bai, J. Bai, G. Pan, Y. Zhu, Y. Zhai, H. Shao, X. Chen, B. Dong and H. Zhang, *Nanotechnology*, 2017, **29**, 085705.
119 L. Wang, Y. Wang, T. Xu, H. Liao, C. Yao, Y. Liu, Z. Li, Z. Chen, D. Pan and L. Sun, *Nat. Commun.*, 2014, **5**, 5357.
120 S. Qu, D. Zhou, D. Li, W. Ji, P. Jing, D. Han, L. Liu, H. Zeng and D. Shen, *Adv. Mater.*, 2016, **28**, 3516–3521.
121 J. Yang, Z. Ren, Z. Xie, Y. Liu, C. Wang, Y. Xie, Q. Peng, B. Xu, W. Tian and F. Zhang, *Angew. Chem., Int. Ed.*, 2017, **56**, 880–884.
122 Q. Zhao, C. Huang and F. Li, *Chem. Soc. Rev.*, 2011, **40**, 2508–2524.
123 A. Köhler, J. S. Wilson and R. H. Friend, *Adv. Mater.*, 2002, **14**, 701–707.
124 Y. Gong, G. Chen, Q. Peng, W. Z. Yuan, Y. Xie, S. Li, Y. Zhang and B. Z. Tang, *Adv. Mater.*, 2015, **27**, 6195–6201.
125 O. Bolton, K. Lee, H.-J. Kim, K. Y. Lin and J. Kim, *Nat. Chem.*, 2011, **3**, 205.
126 G.-P. Yong, Y.-M. Zhang, W.-L. She and Y.-Z. Li, *J. Mater. Chem.*, 2011, **21**, 18520–18522.
127 W. Zhao, Z. He, J. W. Lam, Q. Peng, H. Ma, Z. Shuai, G. Bai, J. Hao and B. Z. Tang, *Chem*, 2016, **1**, 592–602.
128 R. Schmidt, C. Krasselt, C. Göhler and C. von Borczyskowski, *ACS Nano*, 2014, **8**, 3506–3521.
129 Y. Deng, D. Zhao, X. Chen, F. Wang, H. Song and D. Shen, *Chem. Commun.*, 2013, **49**, 5751–5753.
130 P. Long, Y. Feng, C. Cao, Y. Li, J. Han, S. Li, C. Peng, Z. Li and W. Feng, *Adv. Funct. Mater.*, 2018, **28**, 1800791.
131 S. Hirata, *J. Mater. Chem. C*, 2018, **6**, 11785–11794.
132 Z. Tian, D. Li, E. V. Ushakova, V. G. Maslov, D. Zhou, P. Jing, D. Shen, S. Qu and A. L. Rogach, *Adv. Sci.*, 2018, **5**, 1800795.
133 J. Yang, X. Zhen, B. Wang, X. Gao, Z. Ren, J. Wang, Y. Xie, J. Li, Q. Peng, K. Pu and Z. Li, *Nat. Commun.*, 2018, **9**, 840.
134 Y. Gao, H. Han, W. Lu, Y. Jiao, Y. Liu, X. Gong, M. Xian, S. Shuang and C. Dong, *Langmuir*, 2018, **34**, 12845–12852.
135 Q. Li, M. Zhou, Q. Yang, Q. Wu, J. Shi, A. Gong and M. Yang, *Chem. Mater.*, 2016, **28**, 8221–8227.
136 Z. An, C. Zheng, Y. Tao, R. Chen, H. Shi, T. Chen, Z. Wang, H. Li, R. Deng and X. Liu, *Nat. Mater.*, 2015, **14**, 685.

137 P. C. Hsu and H. T. Chang, *Chem. Commun.*, 2012, **48**, 3984–3986.
138 S. Mitra, S. Chandra, T. Kundu, R. Banerjee, P. Pramanik and A. Goswami, *RSC Adv.*, 2012, **2**, 12129.
139 T.-T. Win-Shwe and H. Fujimaki, *Int. J. Mol. Sci.*, 2011, **12**, 6267–6280.
140 S. Sahu, B. Behera, T. K. Maiti and S. Mohapatra, *Chem. Commun.*, 2012, **48**, 8835–8837.
141 Y. Qin, Z. W. Zhou, S. T. Pan, Z. X. He, X. Zhang, J. X. Qiu, W. Duan, T. Yang and S. F. Zhou, *Toxicology*, 2015, **327**, 62–76.
142 B. De and N. Karak, *J. Mater. Chem. A*, 2017, **5**, 1826–1859.
143 S. Kalytchuk, Y. Wang, K. Polakova and R. Zboril, *ACS Appl. Mater. Interfaces*, 2018, **10**, 29902–29908.
144 Z. Song, T. Lin, L. Lin, S. Lin, F. Fu, X. Wang and L. Guo, *Angew. Chem., Int. Ed.*, 2016, **55**, 2773–2777.
145 L. Xiao and H. Sun, *Nanoscale Horiz.*, 2018, **3**, 565–597.
146 M. Li, Y. Feng, Q. Tian, W. Yao, L. Liu, X. Li, H. Wang and W. Wu, *Dalton Trans.*, 2018, **47**, 11264–11271.
147 L. Wang, H. Dong, Y. Li, R. Liu, Y. F. Wang, H. K. Bisoyi, L. D. Sun, C. H. Yan and Q. Li, *Adv. Mater.*, 2015, **27**, 2065–2069.
148 Y. Liu, L. Zhou, Y. Li, R. Deng and H. Zhang, *Nanoscale*, 2017, **9**, 491–496.
149 K. Jiang, Y. Wang, X. Gao, C. Cai and H. Lin, *Angew. Chem., Int. Ed.*, 2018, **57**, 6216–6220.
150 K. Jiang, Y. Wang, C. Cai and H. Lin, *Adv. Mater.*, 2018, **30**, 1800783.
151 C. Lin, Y. Zhuang, W. Li, T. Zhou and R.-J. Xie, *Nanoscale*, 2019, **11**, 6584–6590.
152 Z. Wang, P. Long, Y. Feng, C. Qin and W. Feng, *RSC Adv.*, 2017, **7**, 2810–2816.
153 A. Zhu, Q. Qu, X. Shao, B. Kong and Y. Tian, *Angew. Chem., Int. Ed.*, 2012, **51**, 7185–7189.
154 W. Shi, X. Li and H. Ma, *Angew. Chem., Int. Ed.*, 2012, **51**, 6432–6435.
155 Z. L. Wu, M. X. Gao, T. T. Wang, X. Y. Wan, L. L. Zheng and C. Z. Huang, *Nanoscale*, 2014, **6**, 3868–3874.
156 Y. Yang, W. Kong, H. Li, J. Liu, M. Yang, H. Huang, Y. Liu, Z. Wang, Z. Wang, T. K. Sham, J. Zhong, C. Wang, Z. Liu, S. T. Lee and Z. Kang, *ACS Appl. Mater. Interfaces*, 2015, **7**, 27324–27330.
157 X. Cui, Y. Wang, J. Liu, Q. Yang, B. Zhang, Y. Gao, Y. Wang and G. Lu, *Sens. Actuators, B*, 2017, **242**, 1272–1280.
158 L. Wang, *Liq. Cryst.*, 2016, **43**, 2062–2078.
159 X. Miao, D. Qu, D. Yang, B. Nie, Y. Zhao, H. Fan and Z. Sun, *Adv. Mater.*, 2018, **30**, 1704740.
160 Z. Wang, F. Yuan, X. Li, Y. Li, H. Zhong, L. Fan and S. Yang, *Adv. Mater.*, 2017, **29**, 1702910.
161 S. Lu, L. Sui, J. Liu, S. Zhu, A. Chen, M. Jin and B. Yang, *Adv. Mater.*, 2017, **29**, 1603443.
162 Z. Luo, G. Qi, K. Chen, M. Zou, L. Yuwen, X. Zhang, W. Huang and L. Wang, *Adv. Funct. Mater.*, 2016, **26**, 2739–2744.
163 M. Vazquez-Nakagawa, L. Rodriguez-Perez, M. A. Herranz and N. Martin, *Chem. Commun.*, 2016, **52**, 665–668.
164 H. K. Bisoyi and Q. Li, *Angew. Chem., Int. Ed.*, 2016, **55**, 2994–3010.
165 L. Wang, D. Chen, K. G. Gutierrez-Cuevas, H. K. Bisoyi, J. Fan, R. S. Zola, G. Li, A. M. Urbas, T. J. Bunning and D. A. Weitz, *Mater. Horiz.*, 2017, **4**, 1190–1195.
166 K. Soai, T. Shibata, H. Morioka and K. Choji, *Nature*, 1995, **378**, 767.
167 L. Zhang, M. Wang, L. Wang, D.-K. Yang, H. Yu and H. Yang, *Liq. Cryst.*, 2016, **43**, 750–757.
168 H. Wang, B. Liu, L. Wang, X. Chen, Z. Chen, Y. Qi, G. Cui, H. Xie, Y. Zhang and Z. Liu, *ACS Nano*, 2018, **12**, 6443–6451.
169 L. Wang, A. M. Urbas and Q. Li, *Adv. Mater.*, 2018, 1801335.
170 L. Wang and Q. Li, *Adv. Funct. Mater.*, 2016, **26**, 10–28.
171 L. Wang, H. K. Bisoyi, Z. Zheng, K. G. Gutierrez-Cuevas, G. Singh, S. Kumar, T. J. Bunning and Q. Li, *Mater. Today*, 2017, **20**, 230–237.
172 L. Wang, D. Huang, L. Lam and Z. Cheng, *Liq. Cryst. Today*, 2017, **26**, 85–111.
173 J. Roose, B. Z. Tang and K. S. Wong, *Small*, 2016, **12**, 6495–6512.
174 N. Suzuki, Y. Wang, P. Elvati, Z. B. Qu, K. Kim, S. Jiang, E. Baumeister, J. Lee, B. Yeom, J. H. Bahng, J. Lee, A. Violi and N. A. Kotov, *ACS Nano*, 2016, **10**, 1744–1755.
175 F. Li, Y. Li, X. Yang, X. Han, Y. Jiao, T. Wei, D. Yang, H. Xu and G. Nie, *Angew. Chem., Int. Ed.*, 2018, **57**, 2377–2382.
176 Y. Zhang, L. Hu, Y. Sun, C. Zhu, R. Li, N. Liu, H. Huang, Y. Liu, C. Huang and Z. Kang, *RSC Adv.*, 2016, **6**, 59956–59960.
177 E. Arad, S. K. Bhunia, J. Jopp, S. Kolusheva, H. Rapaport and R. Jelinek, *Adv. Thermoelectr.*, 2018, **1**, 1800006.
178 A. Ghosh, B. Parasar, T. Bhattacharyya and J. Dash, *Chem. Commun.*, 2016, **52**, 11159–11162.
179 M. Zhang, L. Hu, H. Wang, Y. Song, Y. Liu, H. Li, M. Shao, H. Huang and Z. Kang, *Nanoscale*, 2018, **10**, 12734–12742.
180 L. Dong, Y. Feng, L. Wang and W. Feng, *Chem. Soc. Rev.*, 2018, **47**, 7339–7368.
181 C. Hu, C. Yu, M. Li, X. Wang, Q. Dong, G. Wang and J. Qiu, *Chem. Commun.*, 2015, **51**, 3419–3422.
182 S. Gao, Y. Chen, H. Fan, X. Wei, C. Hu, L. Wang and L. Qu, *J. Mater. Chem. A*, 2014, **2**, 6320.
183 H. Li, X. He, Z. Kang, H. Huang, Y. Liu, J. Liu, S. Lian, C. H. Tsang, X. Yang and S. T. Lee, *Angew. Chem., Int. Ed.*, 2010, **49**, 4430–4434.
184 H. Wang, J. Zhuang, D. Velado, Z. Wei, H. Matsui and S. Zhou, *ACS Appl. Mater. Interfaces*, 2015, **7**, 27703–27712.
185 A. Aghamali, M. Khosravi, H. Hamishehkar, N. Modirshahla and M. A. Behnajady, *J. Lumin.*, 2018, **201**, 265–274.
186 H. Zhang, H. Huang, H. Ming, H. Li, L. Zhang, Y. Liu and Z. Kang, *J. Mater. Chem.*, 2012, **22**, 10501.
187 J. Ke, X. Li, Q. Zhao, B. Liu, S. Liu and S. Wang, *J. Colloid Interface Sci.*, 2017, **496**, 425–433.
188 T. F. Yeh, C. Y. Teng, S. J. Chen and H. Teng, *Adv. Mater.*, 2014, **26**, 3297–3303.
189 J. Liu, Y. Liu, N. Liu, Y. Han, X. Zhang, H. Huang, Y. Lifshitz, S.-T. Lee, J. Zhong and Z. Kang, *Science*, 2015, **347**, 970–974.
190 G. Zhang, Q. Ji, Z. Wu, G. Wang, H. Liu, J. Qu and J. Li, *Adv. Funct. Mater.*, 2018, **28**, 1706462.

191 L. Cao, S. Sahu, P. Anilkumar, C. E. Bunker, J. Xu, K. A. Fernando, P. Wang, E. A. Guliants, K. N. Tackett, 2nd and Y. P. Sun, *J. Am. Chem. Soc.*, 2011, **133**, 4754–4757.
192 H. Li, X. Zhang and D. R. MacFarlane, *Adv. Energy Mater.*, 2015, **5**, 1401077.
193 R. Liu, H. Huang, H. Li, Y. Liu, J. Zhong, Y. Li, S. Zhang and Z. Kang, *ACS Catal.*, 2013, **4**, 328–336.
194 F. Qin, J. Tong, R. Ge, B. Luo, F. Jiang, T. Liu, Y. Jiang, Z. Xu, L. Mao and W. Meng, *J. Mater. Chem. A*, 2016, **4**, 14017–14024.
195 D. Dou, J. Duan, Y. Zhao, B. He and Q. Tang, *Electrochim. Acta*, 2018, **275**, 275–280.
196 J. Briscoe, A. Marinovic, M. Sevilla, S. Dunn and M. Titirici, *Angew. Chem., Int. Ed.*, 2015, **54**, 4463–4468.
197 R. Kang, S. Park, Y. K. Jung, D. C. Lim, M. J. Cha, J. H. Seo and S. Cho, *Adv. Energy Mater.*, 2018, **8**, 1702165.
198 H. Choi, S.-J. Ko, Y. Choi, P. Joo, T. Kim, B. R. Lee, J.-W. Jung, H. J. Choi, M. Cha and J.-R. Jeong, *Nat. Photonics*, 2013, **7**, 732.
199 H. KrishnaáBisoyi, *Chem. Commun.*, 2015, **51**, 15039–15042.
200 T. Liu, K. Yu, L. Gao, H. Chen, N. Wang, L. Hao, T. Li, H. He and Z. Guo, *J. Mater. Chem. A*, 2017, **5**, 17848–17855.
201 V. Strauss, K. Marsh, M. D. Kowal, M. El-Kady and R. B. Kaner, *Adv. Mater.*, 2018, **30**, 1704449.
202 X. Zhao, M. Li, H. Dong, Y. Liu, H. Hu, Y. Cai, Y. Liang, Y. Xiao and M. Zheng, *ChemSusChem*, 2017, **10**, 2626–2634.
203 J. S. Wei, C. Ding, P. Zhang, H. Ding, X. Q. Niu, Y. Y. Ma, C. Li, Y. G. Wang and H. M. Xiong, *Adv. Mater.*, 2019, **31**, 1806197.
204 C. Cao, Y. Li, Y. Feng, P. Long, H. An, C. Qin, J. Han, S. Li and W. Feng, *J. Mater. Chem. A*, 2017, **5**, 22519–22526.
205 C. Cao, Y. Li, Y. Feng, C. Peng, Z. Li and W. Feng, *Energy Storage Mater.*, 2019, **19**, 401–407.
206 C. Ma, K. Dai, H. Hou, X. Ji, L. Chen, D. G. Ivey and W. Wei, *Adv. Sci.*, 2018, **5**, 1700996.
207 Y. Hu, W. Chen, T. Lei, B. Zhou, Y. Jiao, Y. Yan, X. Du, J. Huang, C. Wu, X. Wang, Y. Wang, B. Chen, J. Xu, C. Wang and J. Xiong, *Adv. Energy Mater.*, 2019, **9**, 1802955.
208 Y. Yang, X. Ji, M. Jing, H. Hou, Y. Zhu, L. Fang, X. Yang, Q. Chen and C. E. Banks, *J. Mater. Chem. A*, 2015, **3**, 5648–5655.
209 M. Chalfie, Y. Tu, G. Euskirchen, W. W. Ward and D. C. Prasher, *Science*, 1994, **263**, 802–805.
210 L. Yang, W. Jiang, L. Qiu, X. Jiang, D. Zuo, D. Wang and L. Yang, *Nanoscale*, 2015, **7**, 6104–6113.
211 Y. Zhang, Y. Shen, X. Teng, M. Yan, H. Bi and P. C. Morais, *ACS Appl. Mater. Interfaces*, 2015, **7**, 10201–10212.
212 X. Wu, S. Sun, Y. Wang, J. Zhu, K. Jiang, Y. Leng, Q. Shu and H. Lin, *Biosens. Bioelectron.*, 2017, **90**, 501–507.
213 L. Wang, B. Wu, W. Li, Z. Li, J. Zhan, B. Geng, S. Wang, D. Pan and M. Wu, *J. Mater. Chem. B*, 2017, **5**, 5355–5361.
214 H. Dong, W. Dai, H. Ju, H. Lu, S. Wang, L. Xu, S. F. Zhou, Y. Zhang and X. Zhang, *ACS Appl. Mater. Interfaces*, 2015, **7**, 11015–11023.
215 L. Wang, W. He, X. Xiao, F. Meng, Y. Zhang, P. Yang, L. Wang, J. Xiao, H. Yang and Y. Lu, *Small*, 2012, **8**, 2189–2193.
216 H. Tao, K. Yang, Z. Ma, J. Wan, Y. Zhang, Z. Kang and Z. Liu, *Small*, 2012, **8**, 281–290.
217 Y. W. Bao, X. W. Hua, Y. H. Li, H. R. Jia and F. G. Wu, *ACS Appl. Mater. Interfaces*, 2018, **10**, 1544–1555.
218 Q. Liu, S. Xu, C. Niu, M. Li, D. He, Z. Lu, L. Ma, N. Na, F. Huang and H. Jiang, *Biosens. Bioelectron.*, 2015, **64**, 119–125.
219 M. Zheng, S. Ruan, S. Liu, T. Sun, D. Qu, H. Zhao, Z. Xie, H. Gao, X. Jing and Z. Sun, *ACS Nano*, 2015, **9**, 11455–11461.
220 D. Schmaljohann, *Adv. Drug Delivery Rev.*, 2006, **58**, 1655–1670.
221 S. C. Owen, D. P. Chan and M. S. Shoichet, *Nano Today*, 2012, **7**, 53–65.
222 A. Akbarzadeh, R. Rezaei-Sadabady, S. Davaran, S. W. Joo, N. Zarghami, Y. Hanifehpour, M. Samiei, M. Kouhi and K. Nejati-Koshki, *Nanoscale Res. Lett.*, 2013, **8**, 102.
223 P. Pierrat, R. Wang, D. Kereselidze, M. Lux, P. Didier, A. Kichler, F. Pons and L. Lebeau, *Biomaterials*, 2015, **51**, 290–302.
224 L. Wang, X. Wang, A. Bhirde, J. Cao, Y. Zeng, X. Huang, Y. Sun, G. Liu and X. Chen, *Adv. Healthcare Mater.*, 2014, **3**, 1203–1209.
225 A. R. Chowdhuri, S. Tripathy, C. Haldar, S. Roy and S. K. Sahu, *J. Mater. Chem. B*, 2015, **3**, 9122–9131.
226 Q. Zeng, D. Shao, X. He, Z. Ren, W. Ji, C. Shan, S. Qu, J. Li, L. Chen and Q. Li, *J. Mater. Chem. B*, 2016, **4**, 5119–5126.
227 J. Tang, B. Kong, H. Wu, M. Xu, Y. Wang, Y. Wang, D. Zhao and G. Zheng, *Adv. Mater.*, 2013, **25**, 6569–6574.
228 T. Feng, X. Ai, G. An, P. Yang and Y. Zhao, *ACS Nano*, 2016, **10**, 4410–4420.
229 D. W. Zheng, B. Li, C. X. Li, J. X. Fan, Q. Lei, C. Li, Z. Xu and X. Z. Zhang, *ACS Nano*, 2016, **10**, 8715–8722.
230 L. Wang and Q. Li, *Chem. Soc. Rev.*, 2018, **47**, 1044–1097.
231 J. Duan, Y. Zhao, B. He and Q. Tang, *Electrochim. Acta*, 2018, **278**, 204–209.
232 L. Shi, J. H. Yang, H. B. Zeng, Y. M. Chen, S. C. Yang, C. Wu, H. Zeng, O. Yoshihito and Q. Zhang, *Nanoscale*, 2016, **8**, 14374–14378.